Depression of the superconducting transition temperature by magnetic impurities: Effect of Kondo resonance in the f density of states

N. E. Bickers* and G. E. Zwicknagl†
Laboratory of Atomic and Solid State Physics, Cornell University, Ithaca, New York 14853
(Received 13 July 1987)

A new formulation is presented for the calculation of superconducting T_c depression by dilute Ce impurities. The treatment is based on the finite-temperature large-degeneracy expansion for the degenerate-orbital Anderson model. The results may be simply interpreted in terms of resonant structure in the one- and two-body scattering amplitudes; the resonance scale, T_0, may, in principle, be measured directly by inverse-photoemission studies of the f density of states. The initial slope of the depression curve $(-dT_c/dC)\,|_{C=0}$ depends solely on the ratio T_0/T_{c0}, with T_{c0} the pure-metal transition temperature. The maximum initial slope is anomalously large in comparison with typical values for nonresonant magnetic impurity scattering. For an orbital degeneracy $N=6$, maximal depression occurs for $T_0 \simeq 5T_{c0}$.

I. INTRODUCTION

The presence of magnetic impurities in a superconducting host strongly reduces the transition temperature T_c. This suppression of superconductivity results from the breaking of Cooper pairs by conduction-electron scattering. Central to the understanding of T_c depression is, therefore, a general theory for the interaction of conduction electrons with a magnetic impurity. In the normal state, this interaction leads to characteristic low-temperature anomalies in many physical properties (the so-called "Kondo effect").

In the last five years, a simply unifying picture has been developed for understanding normal-state experiments in dilute magnetic alloys. The central concept is the existence of a narrow many-body resonance just above the Fermi level in the one-electron excitation spectrum. The position of this "Kondo resonance" relative to the Fermi level, $k_B T_0$, sets the energy with which all low-temperature properties scale. Several satisfactory mathematical formalisms have been developed which permit the quantitative calculation of normal-state properties over the entire range of reduced temperature T/T_0.[1,2] These techniques have provided a complete description of normal-state properties in the alloy $(La,Ce)B_6$.[1] In contrast, a quantitative treatment of the Kondo resonance has not been incorporated in previous theories for T_c depression.

The successful description of normal-state properties leads us to reexamine the influence of magnetic impurities on the superconducting transition temperature T_c. The depression of T_c is determined by normal-state properties in the vicinity of the pure-host transition temperature T_{c0}. The present treatment is an extension of the "noncrossing approximation," a thermodynamically consistent diagrammatic approximation, to the superconducting state in the vicinity of the transition. This approximation quantitatively describes normal-state behavior over essentially the entire range of T/T_0. For simplicity, we restrict attention to a Ce impurity in a superconducting host. The physical assumption is that Cooper pairs are formed from the conduction electrons of the host, and that the impurity f electrons do not participate in superconductivity. In addition, we consider only conventional s-wave superconductivity. The formal expansion parameter is $1/N$, with N the f-orbital degeneracy of the impurity. To leading order in $1/N$, pair breaking is due to magnetic scattering of conduction electrons from the impurity. This contribution vanishes for low temperature, since the magnetic moment of the impurity is quenched by the Kondo effect. The compensation of the magnetic moment, which is reflected in the disappearance of magnetic scattering, is accompanied by significant changes in the electronic system. In particular, a strong local repulsion develops between conduction electrons with antiparallel spins. This repulsion counteracts the phonon-mediated attraction and leads to a weakening of Cooper pairing. For $T_{c0} \ll T_0$, the transition temperature is reduced by this pair-weakening effect, rather than by pair breaking.

The organization of this paper is as follows. In Sec. II we briefly review the qualitative features of dilute magnetic alloys in the normal and superconducting states and summarize the results of previous calculations of T_c depression. We present an overview of our own results in Sec. III; this section may be of greatest interest to the casual reader. A general expression for the initial slope of T_c depression, $(-dT_c/dC)\,|_{C=0}$, is derived within the quasiclassical approach to superconductivity in Sec. IV. In Sec. V we introduce our model for impurity scattering in detail and summarize the relevant notation. The scattering amplitudes for this model are computed formally in Sec. VI. Numerical results for the one- and two-particle scattering amplitudes and the depression rate of T_c are discussed at length in Sec. VII. In Sec. VIII we offer a summary of our results and comment on the prospects for future work in this area.

We add a final cautionary remark: Although we calculate a measurable effect—the depression of T_c by magnetic impurities—the present paper does not contain

a comparison of our theoretical prediction with experimental results. We are not aware of any complete set of data which would allow such a quantitative test of our theory. There is, of course, a large accumulation of data on T_c depression in various alloys; however, in no case has the Kondo temperature been determined independently by normal-state measurements. The Kondo temperature has conventionally been determined by fitting measurements of T_c directly to the highly successful theory of Müller-Hartmann and Zittartz (MHZ).[3] We hope that discrepancies between our results and those of MHZ will stimulate experimentalists working in this area to perform additional measurements on the normal and superconducting states.

II. REVIEW

Current understanding of magnetic impurities in metals is based largely on the Anderson model.[4] The simplest Anderson Hamiltonian takes the form

$$H_A=\sum_{\mathbf{k},\sigma}\varepsilon_k n_{\mathbf{k}\sigma}+\varepsilon_f\sum_{\sigma}n_{\sigma}+V\sum_{\mathbf{k},\sigma}(c^{\dagger}_{\mathbf{k}\sigma}f_{\sigma}+\text{H.c.})+Un_{\uparrow}n_{\downarrow}\ . \tag{2.1}$$

Here, ε_f is the energy of a localized orbital, U is the Coulomb energy resulting from double orbital occupancy, and V is the hybridization integral between localized states and conduction states with dispersion ε_k. The local level broadening due to hybridization is just

$$\Gamma=\pi N(0)V^2\ , \tag{2.2}$$

with $N(0)$ the single-spin density of conduction states at the Fermi level. Possible configurations of the impurity orbital are f^0, f^1, and f^2.

The simple Hamiltonian in Eq. (2.1) may be generalized to describe more complex impurity configurations. Such a generalization is necessary to describe the local angular momentum structure of the lanthanides, in which spin-orbit coupling is strong. In this case, impurity orbitals must be labeled by total angular momentum, rather than spin. The simplest lanthanides to treat are Ce (configurations f^0, f^1, and f^2) and its particle-hole analog Yb (f^{14}, f^{13}, and f^{12}). In the following discussion, we specialize to Ce for simplicity.

A. Three regimes for normal metals containing magnetic impurities

In the lanthanides, the Coulomb repulsion U is of the order of 5–10 eV. Although the f^2 configuration in Ce systems may be detected in inverse photoemission experiments, it is largely irrelevant to the physics of low-energy processes.[5] Hence, it is a reasonable approximation to set $U=\infty$, eliminating all configurations but f^0 and f^1. Assuming a relatively structureless band, the properties of the system are then determined solely by the position and width of the f^1 configuration. Three qualitatively distinct regimes are possible.

(1) $\varepsilon_f/\Gamma\gg 1$; this may be called the "empty impurity regime." The f^0 configuration dominates on energetic grounds. The properties of the system are dull, i.e., the scattering is nonmagnetic in character.

(2) $-\varepsilon_f/\Gamma\gg 1$; this may be called the "Kondo regime." The system is dominated by the f^1 configuration and may be alternatively described by an antiferromagnetic spin, or spin-orbital, exchange Hamiltonian with localized impurity–conduction-band coupling. The exchange constant for $U=\infty$ is just

$$J=V^2/\varepsilon_f<0\ . \tag{2.3}$$

In this regime, the scattering is magnetic in character. At high temperatures, the impurity susceptibility is Curie-like, indicating free-spin behavior. As the temperature is lowered, the Kondo effect begins to manifest itself. The Kondo effect is the screening of a local magnetic moment by antiferromagnetic interaction with conduction electrons. Below a characteristic Kondo scale T_0 (to be defined precisely in Sec. III), the susceptibility becomes Pauli-like, and the specific heat becomes linear in temperature; such behavior characterizes a Fermi liquid. The formation of a spin-compensated ground state is accompanied by strong resonant scattering near the Fermi surface. This resonant scattering leads to transport anomalies in the impurity resistivity, thermopower and thermal conductivity.[2]

(3) $|\varepsilon_f/\Gamma|\leq 1$; this is the "mixed-valent" or "valence-fluctuation" regime. In this case, the configurations f^0 and f^1 are approximately degenerate. The properties of the system cross over smoothly from the behavior of regime (2) to that of regime (1) as the f^1 level is raised through the f^0 level. In the mixed-valent regime, the impurity may no longer be described as a long-lived spin (mathematically, the Schrieffer-Wolff transformation[6] becomes invalid). Alternatively, the spin must be viewed as a transient object with a characteristic spin-fluctuation lifetime.

B. Effect of magnetic impurities on T_c

The effect of impurities on superconductivity is expected to differ in the three regimes discussed in Sec. III A. In the *empty impurity regime,* the ground state is nonmagnetic. Cooper pairs may be formed from electrons in degenerate time-reversed states; however, hybridization with highly correlated impurity levels induces an effective repulsion between conduction electrons with opposite spin. This repulsion grows with increasing impurity concentration, reducing the attractive pairing interaction responsible for superconductivity. "Pair weakening" by resonant impurity scattering has been treated within Hartree-Fock approximations by Kaiser,[7] Shiba,[7] and Schlottmann.[8] According to Kaiser's theory, T_c is a modified exponential function of impurity concentration. Such a form is expected since the decrease in the effective pairing interaction is nearly linear in concentration. Properties such as the normalized specific heat discontinuity, $\Delta C/C\,|_{T_c}$, obey the Bardeen-Cooper-Schrieffer (BCS) law of corresponding states. The Hartree-Fock treatment is limited in validity to systems with small Coulomb repulsion,[8] i.e., $U/\Gamma\ll 1$; this condition is not fulfilled in lanthanide al-

loys. Nevertheless, Kaiser's theory has yielded a consistent description of lanthanide alloys with large Kondo, or spin-fluctuation, scales (e.g., *Th*Ce).[9] A more-refined theory should yield similar results in this limit.

The *mixed-valent regime* has been the subject of relatively few investigations to date. Since the configurations f^0 and f^1 are nearly degenerate, virtual charge and spin fluctuations are of comparable importance. The transition temperature, specific heat discontinuity, and upper critical field have been computed perturbatively[10] to $O(V^2)$. In addition, the zero-temperature large-degeneracy expansion of Gunnarsson and Schönhammer[11] has been recently extended to the superconducting state.[12]

The *Kondo regime,* in which long-lived impurity spins exist (before quenching sets in), has been the object of especially intense study, which dates from the work of Anderson[13] and Abrikosov and Gor'kov.[14] Anderson demonstrated that stable spins lead to strong T_c depression by breaking the time-reversal invariance of a pure metal. This is a qualitatively different mechanism from the nonmagnetic pair weakening effect described above. In a nonmagnetic system, stable Cooper pairs may be formed from exact time-reversed eigenstates; T_c depression results from a weakened pairing interaction. If the nonmagnetic scattering is also nonresonant, the transition temperature is insensitive to small concentrations of impurities.[15] In perturbation theory, this null result emerges as a cancellation of lifetime effects: while single-electron free-particle states acquire a finite lifetime, dressed Cooper pairs scatter "in tandem," and the overall pair-breaking effect vanishes. In contrast, as shown by Abrikosov and Gor'kov (AG), no such cancellation of one- and two-body effects occurs when impurity scattering is magnetic. The AG treatment is a second-order Born approximation in the exchange constant J; the Kondo effect generates logarithmic divergences in perturbation theory beginning with terms of $O(J^3)$. The AG result is nevertheless expected to remain valid in the limit $JN(0)\rightarrow 0$, when the Kondo scale T_0 is exponentially smaller than the pure-metal transition temperature T_{c0}. AG theory has been extended to compute the specific heat discontinuity $\Delta C/C\mid_{T_c}$.[16] The predicted dependence on T_c violates the BCS law of corresponding states. This dependence has been observed in lanthanide systems such as $(La,Gd)Al_2$, in which the effective exchange integral J is positive and no Kondo effect occurs.[17]

The presence of the Kondo effect greatly complicates the treatment of T_c depression. From a purely technical viewpoint, an approach which avoids the unphysical divergences of low-order perturbation theory in the exchange constant is required. A minimal constraint on the theory is that it reproduce the second-order Born approximation of AG in the limit of a vanishingly small Kondo scale, $T_0/T_{c0}\rightarrow 0$. On the other hand, it must incorporate the opposing tendencies which exist when the Kondo scale and pure-metal transition temperature are comparable. In the first place, formation of the Kondo ground state is accompanied by resonant one-electron scattering near the Fermi surface; in a system with stiff impurity moments, such scattering would lead to high normal-state resistivity just above T_c and anomalously large T_c depression (due to lack of time-reversal invariance). On the other hand, the effective moments in a Kondo system are not stiff; rather they decrease as the many-body ground state develops, tending to zero at temperatures below T_0. This second effect makes impurity scattering increasingly nonmagnetic at low temperatures and tends to diminish pair breaking when T_0 and T_{c0} are comparable.

Thus, as the ratio T_0/T_{c0} increases from zero, it is plausible that the initial slope of T_c depression, $(-dT_c/dC)\mid_{C=0}$, initially increases, reaches a maximum when the ratio is of order unity, and finally decreases toward zero as the Kondo scale becomes large. The existence of a singlet Kondo ground state implies that only pair weakening should be present for $T_0/T_{c0}\gg 1$.

C. Previous theories for the Kondo regime: MHZ and MIN

A theory which nonperturbatively incorporates the Kondo effect in the study of T_c depression was developed in the early 1970s by Müller-Hartmann and Zittartz (MHZ).[18] Their calculation assumes the existence of a stable local spin and is an extension to the superconducting state of the Green's function decoupling scheme of Nagaoka and Hamann.[19] Within this approximation, exact expressions may be derived for $(-dT_c/dC)\mid_{C=0}$ and $\Delta C/C\mid_{T_c}$. Both properties are functions only of the ratio T_K/T_{c0}, with T_K the "Kondo temperature" of Nagaoka-Hamann theory. Maximum initial depression occurs for $T_K\approx 12T_{c0}$ and takes the value

$$(-dT_c/dC)\mid_{C=0}^{\max}\approx 0.125N(0)^{-1}\ . \tag{2.4}$$

The location and size of the maximum are almost independent of the impurity spin magnitude. The initial depression curve is roughly Lorentzian in $\ln(T_K/T_{c0})$ with half-width $\pi(S+\frac{1}{2})$.[20] In the limit $T_K/T_{c0}\rightarrow 0$, the result of AG theory is recovered. Surprisingly, this result emerges as well in the opposite limit $T_K/T_{c0}\rightarrow\infty$, where the impurity spin is completely quenched.

The Nagaoka-Hamann approximation scheme collapses at temperatures below T_K, yielding nonanalytic features in all physical properties. For example, the calculated normal-state resistivity exhibits a logarithmic saturation,[19] rather than the quadratic behavior of a general Fermi liquid. This shortcoming is expected to invalidate the results of MHZ theory in the Fermi-liquid regime $T_{c0}\ll T_K$.

MHZ theory has been applied with notable success to the alloy (La,Th)Ce.[9] The characteristic temperature of this system may be raised by increasing the concentration of Th. The consistency of predictions for the initial depression in T_c and the specific heat discontinuity provides a partial test of the theory. The agreement is good when the theoretical Kondo scale is small, but fails, as expected, for large values of T_K/T_{c0} (high Th concentra-

tion). Analogous results have been obtained for the systems (La,Y)Ce and (La,Ce)$Sn_{3-x}Pb_x$.[21]

A Fermi-liquid theory for T_c depression has been developed by Matsuura, Ichinose, and Nagaoka (MIN),[22] and independently by Sakurai.[23] Pair weakening occurs through virtual polarization of the Kondo singlet ground state; properties such as the specific heat discontinuity obey the BCS law of corresponding states. This theory is strictly valid only when $T_K/T_{c0} \gg 1$. MIN have attempted to incorporate results of Fermi-liquid theory and high-temperature perturbation theory in an interpolation scheme for $T_{c0} \approx T_K$. This approach is highly problematic, however; the low- and high-temperature scales differ by a factor of order unity, and the interpolation itself is largely arbitrary. For this reason, MIN theory must be viewed as qualitative in nature outside the Fermi-liquid regime.

III. DESCRIPTION AND RESULTS

In this section we present a broad overview of our results. A more complete description of the calculational approach is presented in Secs. IV–VII. We restrict attention to Ce systems; the impurity angular momentum structure is particularly simple in this case, and the relevant configurations are f^0 and f^1. A central concept to be emphasized throughout is the universality of low-temperature properties, including T_c depression, in the Kondo regime. This universality results from the scaling form of the resonant amplitudes for one- and two-electron scattering from impurities.

In the extremely dilute limit, impurity-impurity interactions may be ignored. The energy-dependent amplitude for one-electron scattering takes the simple form $CT_1(\omega)$, with C the dimensionless impurity concentration and T_1 the one-electron t matrix for scattering from a single impurity. The t matrix is indicated schematically in Fig. 1. The total scattering rate $\tau^{-1}(\omega)$ is the dissipative part of this amplitude, i.e.,

$$\tau^{-1}(\omega) = -2C \, \mathrm{Im} T_1(\omega + i0^+) \, . \tag{3.1}$$

A distinguishing feature of magnetic impurity scattering is the strong frequency dependence of the scattering amplitude; in the limit of large on-site correlation ($U \to \infty$), the low-temperature scattering rate exhibits a sharp resonance just above the Fermi surface. The position T_0 of this "Kondo resonance" sets the scale for all low-temperature properties. The growth of the Kondo resonance at low temperatures is indicated in Fig. 2 for a typical choice of parameters (see Table I).

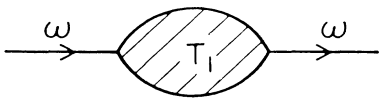

FIG. 1. Schematic representation of the amplitude for one-electron scattering from a single impurity. An electron of energy ω (indicated by the solid line) scatters elastically from the impurity site with energy-dependent amplitude $T_1(\omega)$; the amplitude has both real and imaginary parts.

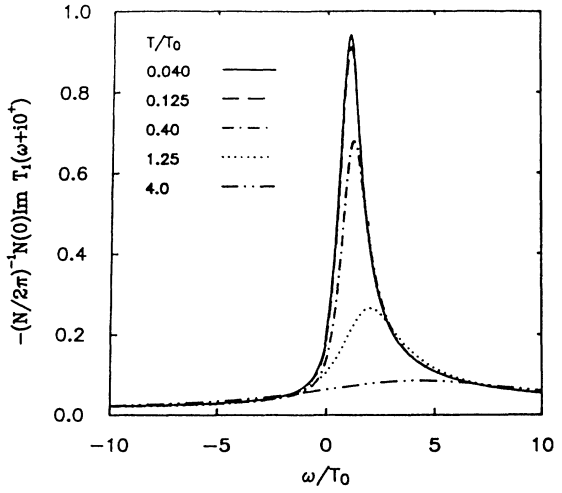

FIG. 2. Growth of the one-electron scattering amplitude with decreasing temperature. The results shown above correspond to the first parameter set in Table I. The impurity degeneracy N is 6. A "Kondo resonance" in the scattering amplitude appears just above the Fermi surface as the temperature is decreased. The position of this resonance at zero temperature T_0 sets the scale for all low-temperature properties.

The description of low-temperature properties is simplified by the universal characteristics of the scattering amplitude. Specifically, the dimensionless quantity $N(0)T_1(\omega)$ is a nearly universal function of the scaled frequency ω/T_0 and the scaled temperature T/T_0. The extent to which this scaling is valid is indicated in Fig. 3 for values of T_0 varying by more than 2 orders of magnitude.

The amplitude for opposite-spin two-electron scattering from an impurity, $T_2(\omega_1,\omega_2;\nu)$, has equally strong

TABLE I. Parameters for calculation of T_c depression. The parameter sets used in calculations of $-dT_c/dC$ are listed below. The magnetic ion has an f^1 ground state with degeneracy $N=6$ and an f^0 excited state: $E(f^1)-E(f^0)=\varepsilon_f<0$. Energies are measured from the Fermi level for the system with an f^0 configuration. The conduction band is centered on the Fermi level and has a Lorentzian profile with half-width D. (A half-width of 3 eV is reasonable for most dilute Ce alloys.) In each case, $\varepsilon_f/D=-0.67$ (an f^0-f^1 separation of 2 eV for $D=3$ eV.) The hybridization width for impurity-conduction electron mixing is Γ. The Kondo scale T_0 is the position of the Fermi surface resonance in the f density of states for $T \to 0$. T_0 may be estimated within a factor of order unity by the expression $T_0 \sim D g^{1/N} e^{-1/Ng}$, where $g=\Gamma/\pi|\varepsilon_f|$. Note that all three parameter sets have been used in studies of normal-state properties as well (Ref. 1).

Parameter set	Γ/D	T_0/D	n_f
1	0.05	4.8×10^{-4}	0.97
2	0.075	5.3×10^{-3}	0.92
3	0.20	1.1×10^{-1}	0.71

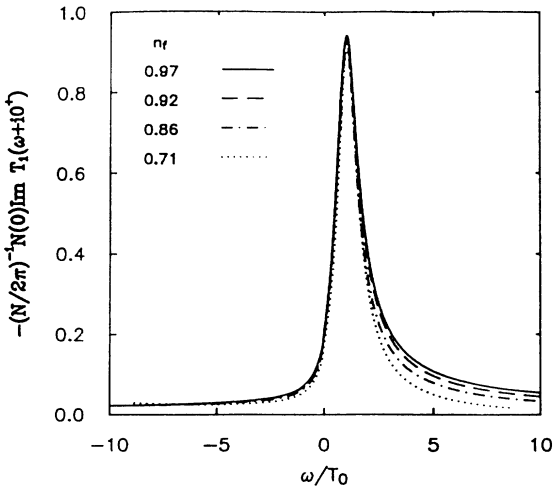

FIG. 3. Single-variable scaling of the one-electron scattering amplitude for $T\to 0$. Parameters are summarized in Table I. For Kondo scales varying by a factor of more than 200, the amplitude exhibits approximate scaling at energies $|\omega| < 2T_0$.

energy dependence. This amplitude is indicated schematically in Fig. 4.

Both elastic ($\nu=0$) and inelastic ($\nu\neq 0$) processes are possible since the impurity–conduction-electron ground state has internal structure and may be polarized; both processes contribute to T_c depression in general. The present calculation retains only elastic (indexed as elast) and "elastic spin-flip" (SF) processes. The second category requires energy transfer $\nu=\omega_2-\omega_1$. Since the same processes enter AG theory,[14] the present calculation may be called an "energy-dependent AG approximation."

The processes relevant to T_c depression involve scattering of electrons with energies distributed symmetrically about the Fermi surface, i.e., with $\omega_1=-\omega_2=\omega$. In this case, the dimensionless quantities $[N(0)]^2T_2^{\rm elast}(\omega)$ and $[N(0)]^2T_2^{\rm SF}(\omega)$ with

$$T_2^{\rm elast}(\omega)=T_2(\omega,-\omega;0)\ ,$$
$$T_2^{\rm SF}(\omega)=T_2(\omega,-\omega;-2\omega) \tag{3.2}$$

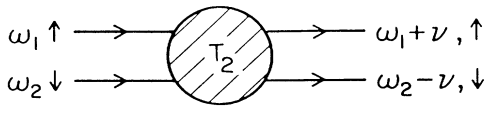

FIG. 4. Schematic representation of the amplitude for opposite-spin two-electron scattering from a single impurity T_2. A spin-up and spin-down electron with energies ω_1 and ω_2 scatter from the impurity, exchanging energy ν. In an *elastic* event, the electrons in the initial and final states have the same energy and spin ($\nu=0$); in an *elastic spin-flip* event, the electrons in the initial and final states have the same energies, but opposite spins ($\nu=\omega_2-\omega_1$).

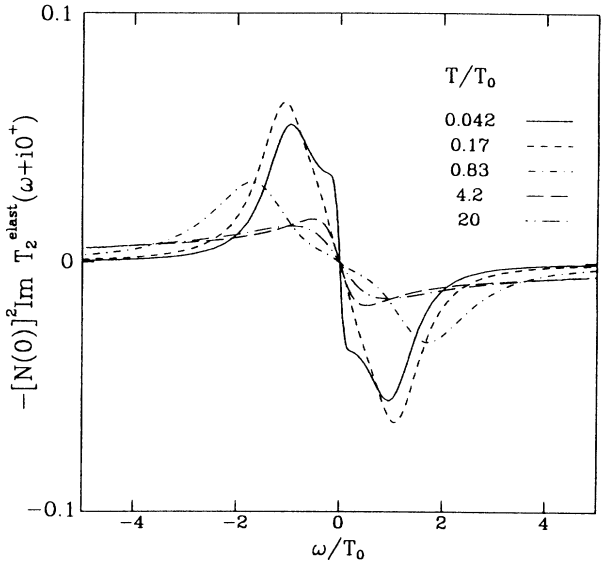

FIG. 5. Temperature dependence of the amplitude for elastic scattering of two electrons, $T_2^{\rm elast}$. The imaginary part of both the elastic and elastic spin-flip amplitudes is odd in frequency. At low temperature, strong resonances appear near $\omega=\pm T_0$; these resonances indicate that electron pairs with energy of order the Kondo scale are strongly scattered by the impurity (just as single electrons are scattered). The shoulders in the lowest-temperature curve for $\omega\to 0^{\pm}$ are an artifact of the approximate solution scheme.

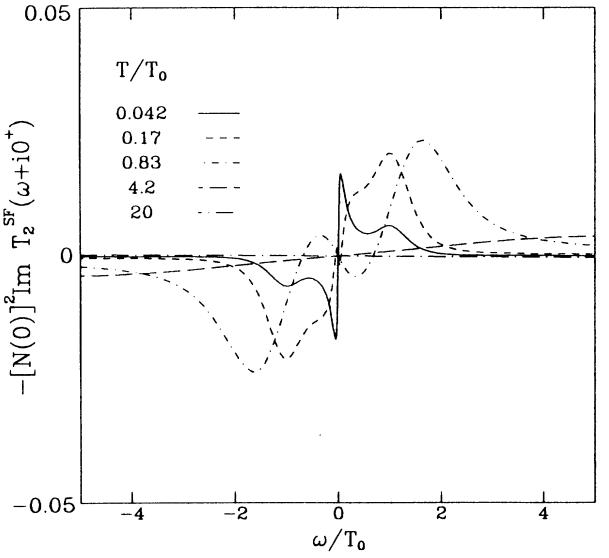

FIG. 6. Temperature dependence of the amplitude for elastic spin-flip scattering of two electrons, $T_2^{\rm SF}$. For $T<T_0$, resonances appear near $\omega=\pm T_0$. These resonances are opposite in sign to those in the elastic amplitude; their weight rapidly diminishes at $T\to 0$. In addition, the lowest-temperature curves exhibit spurious features at zero frequency. As in the case of the elastic amplitude, these features are an artifact of the approximation scheme.

exhibit universal behavior as functions of ω/T_0 and T/T_0, in analogy with the one-body amplitude. The low-temperature growth of the elastic and elastic spin-flip amplitudes is indicated in Figs. 5 and 6; their scaling behavior is illustrated in Figs. 7 and 8. (For the values of parameters, see Table I.) Since the one- and two-body scattering amplitudes scale with characteristic energy T_0, the initial depression of T_c is a nearly universal function of T_0/T_{c0} in the Kondo regime. The contributions to $(-dT_c/dC)\,|_{C=0}$ from the one- and two-body amplitudes are plotted in Fig. 9. The impurity degeneracy $N=2j+1$ is chosen to be 6, the spin-orbit ground-state degeneracy of Ce. The approximate scaling of the depression rate is illustrated in Fig. 10.

The behavior of the calculated $N=6$ depression curve is as follows: maximum depression occurs for $T_0 \approx 5T_{c0}$. This is of the same order as the Kondo model results of MHZ (Ref. 20) and MIN (Ref. 22). The peak depression rate is

$$-(dT_c/dC)\,|^{\max}_{C=0} \approx 0.13N(0)^{-1} \tag{3.3}$$

for the parameter set with maximum impurity valence $n_f(T=0)=0.97$. The peak decreases slightly in height as mixed-valent character increases.

The calculation reported here is least accurate for large values of T_0/T_{c0}. There are two primary sources of error. (1) The calculation is based on the self-consistent large-degeneracy expansion, or noncrossing approximation (NCA), which breaks down at temperatures $T_{c0} \ll T_0$.[24] The characteristic scale for anomalous behavior is, however, quite small in the Kondo regime. This scale may be estimated as[24]

$$T^*_{\rm NCA} \sim \frac{T_0}{N+1}(\pi T_0/\Gamma)^{(N+1)/(N-1)} . \tag{3.4}$$

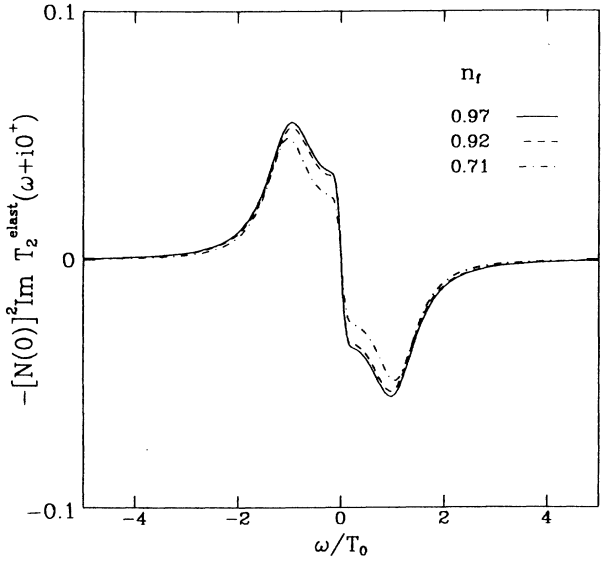

FIG. 7. Single-variable scaling of the elastic amplitude for $T/T_0 \sim 0.04$. The amplitude shows similar scaling at other temperatures. Deviations from scaling are evident in the curve for $n_f=0.71$ (the weakly-mixed-valent regime).

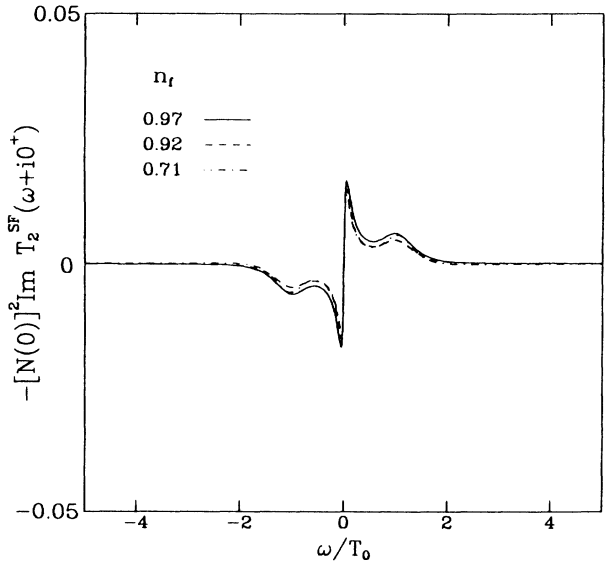

FIG. 8. Single-variable scaling of the elastic spin-flip amplitude for $T/T_0 \sim 0.04$.

Results reported here are limited to the range $T_{c0} \geq T^*_{\rm NCA}$. (2) The approximation of retaining only elastic and elastic spin-flip processes is expected to become invalid as $T_{c0} \to 0$. In this limit, both one- and two-body contributions to $(-dT_c/dC)\,|_{C=0}$ are large and of opposite sign; the inclusion of inelastic two-body

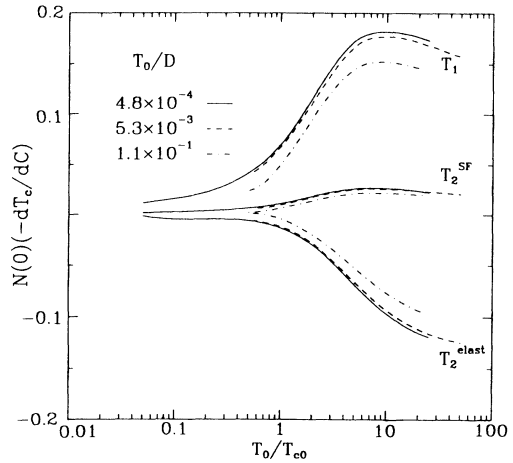

FIG. 9. Contributions to the initial slope of T_c depression from the one- and two-electron scattering amplitudes. The parameters of this plot are summarized in Table I. The strong scattering of single electrons with energy of order T_0 leads to a large initial slope for T_c depression. This effect is opposed by the elastic two-electron contribution, which reflects the increasingly nonmagnetic character of impurity scattering for large T_0/T_{c0}. The elastic spin-flip contribution is small at all temperatures; as in the original AG calculation, the spin-flip amplitude increases the slope of T_c depression. The curves for f valence 0.97 and 0.92 are nearly coincident. This reflects the scaling behavior of the one- and two-electron amplitudes (Figs. 3, 7, and 8). The curves for the weakly-mixed-valent system ($n_f=0.71$) show the expected deviation from scaling.

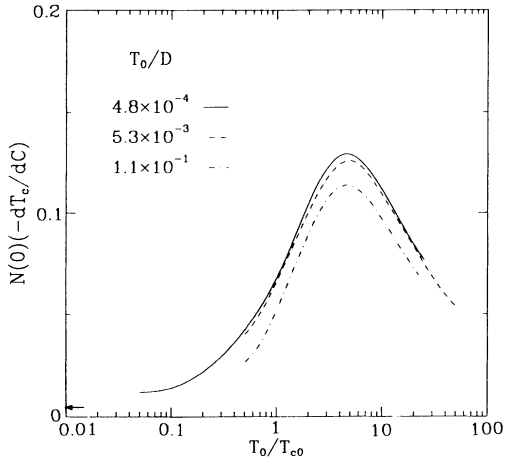

FIG. 10. Total initial slope of T_c depression. The slope is maximized for $T_0/T_{c0}\sim 5$. The peak value for $n_f=0.97$ is ~ 0.13, close to the peak value of 0.125 deduced for the Kondo model in the studies of MHZ (Ref. 18) and MIN (Ref. 22). For $T_0 \ll T_{c0}$, the initial slope is small since resonant one- (and two-) electron scattering near the Fermi surface is weak: The Kondo resonance has not yet developed. For $T_0 \gg T_{c0}$, the initial slope is small even though one-electron scattering is quite strong: Cooper pairs maintain their coherence by scattering in tandem from nonmagnetic centers. The small arrow at the lower left indicates the magnitude of initial T_c depression which follows from a second-order Born approximation neglecting the Kondo effect. Applying Eq. (B18) of Appendix B to the first parameter set in Table I gives $N(0)(-dT_c/dC)\,|_{C=0}=0.0049$.

processes may then be important. For these reasons, the present calculation is insufficient to determine the quantitative form of $(-dT_c/dC)\,|_{C=0}$ for the Fermi-liquid regime $T_{c0} \ll T_0$. Nevertheless, we expect that the determination of the peak position and height will not be significantly affected by inclusion of inelastic processes.

IV. GENERAL EXPRESSION FOR T_c DEPRESSION IN THE DILUTE LIMIT

In the present section we briefly introduce our method for treating superconductivity and write down the equations relating the initial slope of T_c depression, $(-dT_c/dC)\,|_{C=0}$, to scattering by rare-earth impurities. We use the quasiclassical theory of superconductivity.[25] We apply the framework of the theory for small defects in a superconductor[26] and extend it by including the internal dynamics of the scattering center.

The characteristic length and time scales in superconducting phenomena are set by the coherence length $\xi_0=\hbar v_F/\pi T_c$ and the inverse gap frequency Δ^{-1}. Both are very large on the atomic scale determined by the Fermi wave vector k_F^{-1} and the inverse Fermi frequency ε_F^{-1}. The anomalies introduced by resonant scattering from rare-earth impurities also occur at energies $T_0 \ll \varepsilon_F$. The quasiclassical theory of superconductivity is valid only for variations on these coarse-grained scales. At the outset, properties determined by the Fermi wavelength k_F^{-1} and the Fermi energy ε_F are explicitly eliminated from the theory. The advantage gained is a considerable simplification, elegance, and calculational ease. We would like to emphasize that, since the traditional BCS theory is restricted in accuracy to terms of order T_c/ε_F, an advantage of the quasiclassical method is that it acknowledges this fact and eliminates as many intermediate steps as possible.

The quasiclassical theory is based on formal many-body perturbation theory, expressed in terms of the thermodynamic (imaginary time) Green's function $\hat{G}(\mathbf{x},\mathbf{x}';i\omega_n)$; in this case, $\hat{G}$ is a 4×4 matrix which contains the "anomalous" Green's functions in the off-diagonal quadrants. In what follows, only the static limit will be important, and consequently only one frequency, the energy variable, appears as an argument. The central quantity of this theory is the "quasiclassical" or "ξ-integrated" Green's function $\hat{g}$. It is derived from the quasiparticle part of the full propagator

$$\hat{G}(\mathbf{p};i\omega_n)=\int_0^\beta d\tau\, e^{i\omega_n\tau}\begin{bmatrix} \langle\langle c_{\mathbf{p}\sigma}(\tau)c^\dagger_{\mathbf{p}\sigma'}(0)\rangle\rangle & \langle\langle c_{\mathbf{p}\sigma}(\tau)c_{-\mathbf{p}\sigma'}(0)\rangle\rangle \\ \langle\langle c^\dagger_{-\mathbf{p}\sigma}(\tau)c^\dagger_{\mathbf{p}\sigma'}(0)\rangle\rangle & \langle\langle c^\dagger_{-\mathbf{p}\sigma}(\tau)c_{-\mathbf{p}\sigma'}(0)\rangle\rangle \end{bmatrix}, \tag{4.1}$$

$$\langle\langle A(\tau)B(0)\rangle\rangle=-\langle T_\tau A(\tau)B(0)\rangle ,$$

by averaging over the magnitude of the momentum $\mathbf{p}$:

$$\hat{g}(\hat{\mathbf{p}};i\omega_n)=a^{-1}\hat{\tau}_3\int_{-E_c}^{E_c} d\xi_p \hat{G}(\mathbf{p};i\omega_n) , \tag{4.2}$$

where $\xi_p=v_F(p-p_F)$. Here a, v_F, and p_F denote the quasiparticle renormalization factor, the Fermi velocity, and the Fermi wave vector, respectively. The unit vector $\hat{\mathbf{p}}$ defines a direction on the Fermi surface. The formal intermediate cutoff E_c, which satisfies $\varepsilon_F \gg E_c \gg T_c$, can always be eliminated from observables. Finally, $\hat{\tau}_3$ is a 4×4 Pauli matrix with particle-hole indices, i.e.,

$$\hat{\tau}_3=\begin{bmatrix} 1 & 0 \\ 0 & -1 \end{bmatrix} \tag{4.3}$$

with each entry a 2×2 matrix.

The Eilenberger equations, which determine $\hat{g}$, are derived from the Dyson equation for the full Green's function. They take the form of a transportlike equation plus a normalization condition. For homogeneous systems in the static limit, the Eilenberger equations are

$$[i\omega_n\hat{\tau}_3-\hat{\sigma}\{\hat{g}\},\hat{g}(\hat{\mathbf{p}};i\omega_n)]=0 ,$$
$$\hat{g}^2(\hat{p};i\omega_n)=-\pi^2\hat{1} . \tag{4.4}$$

Here $\hat{\sigma}\{\hat{g}\}$ is the quasiclassical self-energy defined as a functional of $\hat{g}$. This self-energy equation provides the order parameter through

$$\Delta(i\sigma_2)=\lambda T\sum_n{}' \int \frac{d\hat{p}}{4\pi}\hat{g}^{12}(\hat{\mathbf{p}};i\omega_n)\ , \tag{4.5}$$

where Δ is the order parameter, σ_2 is a 2×2 Pauli spin matrix, and λ is the BCS coupling constant. A singlet order parameter is assumed for simplicity.

An impurity whose perturbation potential is localized to a scale k_F^{-1} can be incorporated into the quasiclassical theory as a "boundary condition." Conduction-electron scattering from an impurity at site $\mathbf{R}_i$ can be accounted for by a transition matrix element

$$e^{i(\mathbf{k}-\mathbf{k}')\cdot\mathbf{R}_i}\hat{T}(\mathbf{k},\mathbf{k}';i\omega_n)\ . \tag{4.6}$$

The quasiclassical theory exploits the fact that $\hat{T}$ depends on $|\mathbf{k}|$ and $|\mathbf{k}'|$ only near k_F (reflecting the short-range nature of the impurity). To leading order in the ratio $(\xi_0 k_F)^{-1}$, $|\mathbf{k}|$ and $|\mathbf{k}'|$ may be restricted to k_F, leaving only the angular dependence on $\hat{\mathbf{k}}$ and $\hat{\mathbf{k}}'$. This leads to the definition of the quasiclassical t matrix for the impurity at site $\mathbf{R}_i$,

$$\hat{t}(\hat{\mathbf{k}},\hat{\mathbf{k}}';i\omega_n)=a\hat{T}(k_F\hat{\mathbf{k}},k_F\hat{\mathbf{k}}';i\omega_n)\hat{\tau}_3\ . \tag{4.7}$$

An average with respect to the impurity positions leaves only the forward-scattering amplitude $\hat{t}(\hat{\mathbf{k}};i\omega_n)$. The final inhomogeneous equation for the quasiclassical propagator $\hat{g}$ is

$$[i\omega_n\hat{\tau}_3-\hat{\sigma}_{\rm MF}\{\hat{g}\},\hat{g}(\hat{\mathbf{p}};i\omega_n)] =C[\hat{t}(\hat{\mathbf{p}};i\omega_n),\hat{g}_0(\hat{\mathbf{p}};i\omega_n)]\ , \tag{4.8}$$

with $\hat{g}_0$ determined by Eq. (4.4) and $\hat{\sigma}_{\rm MF}$ the mean-field self-energy due to the pairing interaction. C is the dimensionless impurity concentration. This equation holds only to lowest order in C. More generally, $\hat{g}_0$ must be replaced by a dressed $\hat{g}$, with $\hat{t}$ determined self-consistently as a functional of $\hat{g}$.

The superconducting transition temperature of the impure system T_c is obtained from the self-consistency equation (4.5) linearized with respect to the anomalous amplitudes. For a system with an isotropic singlet order parameter and isotropic impurity scattering, one may write quite generally

$$\hat{t}(\hat{\mathbf{k}};i\omega_n)\equiv t(i\omega_n) =\mathrm{Re}\,t_1(i\omega_n)\hat{\mathbb{1}}+i\,\mathrm{Im}\,t_1(i\omega_n)\hat{\tau}_3 +t_2(i\omega_n)(i\sigma_2)\hat{\tau}_1\ , \tag{4.9}$$

where t_1 and t_2 denote the particle-hole diagonal and off-diagonal scattering amplitudes, respectively. It is straightforward to show (see Appendix A) that the initial slope of T_c depression is related to (4.9) by

$$(-dT_c/dC)\,|_{C=0}=-\pi T_{c0}^2\sum_n\left[\frac{\mathrm{sgn}\,\omega_n}{\omega_n^2}\,\mathrm{Im}\,t_1(i\omega_n) +\frac{t_2(i\omega_n)}{\Delta\,|\,\omega_n\,|}\bigg|_{\Delta=0}\right]. \tag{4.10}$$

V. MODEL AND NOTATION

As shown in the preceding section, the calculation of T_c depression in the dilute impurity limit reduces to finding the single-impurity t matrix. In this section a detailed model for impurity scattering is introduced, along with the relevant notation.

The system of conduction electrons interacting with a magnetic impurity is modeled by the infinite-U Anderson Hamiltonian.[4] For a single rare-earth impurity, the complete Hamiltonian takes the form

$$H=H_{\rm band}+H_f+H_{\rm mix}+H_{\rm pair}\ ,$$

where

$$\begin{aligned} H_{\rm band}&=\sum_{\mathbf{k},\sigma}\varepsilon_k n_{\mathbf{k}\sigma}\ ,\\ H_f&=\varepsilon_f\sum_M |M\rangle\langle M|\ ,\\ H_{\rm mix}&=\sum_{k,M}V(k)(c_{kM}^\dagger|M\rangle\langle 0|+\mathrm{H.c.})\ , \end{aligned} \tag{5.1}$$

and

$$H_{\rm pair}=\tfrac{1}{2}\sum_{\mathbf{k},\mathbf{k}',\sigma,\sigma'}U(\mathbf{k},\mathbf{k}')c^\dagger_{-\mathbf{k}\sigma}c^\dagger_{\mathbf{k}'\sigma'}c_{-\mathbf{k}'\sigma}\ .$$

The zero of energy is chosen to be the energy of the noninteracting Fermi sea and an empty impurity orbital. The notation is as follows.

(1) $n_{\mathbf{k}\sigma}=c^\dagger_{\mathbf{k}\sigma}c_{\mathbf{k}\sigma}$, with $c^\dagger_{\mathbf{k}\sigma}$ the creation operator for a plane-wave conduction state of wave vector $\mathbf{k}$, spin σ. An isotropic conduction-band dispersion $\varepsilon_{\mathbf{k}}=\varepsilon_k$ is assumed throughout. All energies are measured relative to the Fermi level. The plane-wave normalization is chosen such that

$$\begin{aligned} &\langle\mathbf{r}\sigma|c^\dagger_{\mathbf{k}\sigma}|0\rangle=e^{i\mathbf{k}\cdot\mathbf{r}}\ ,\\ &\{c_{\mathbf{k}\sigma},c^\dagger_{\mathbf{k}'\sigma'}\}=(2\pi)^3\delta(\mathbf{k}-\mathbf{k}')\delta_{\sigma\sigma'}\ . \end{aligned} \tag{5.2}$$

In formal sums over plane-wave states,

$$\begin{aligned} &\sum_{\mathbf{k},\sigma}\leftrightarrow\sum_\sigma\int\frac{d\mathbf{k}}{(2\pi)^3}\ ,\\ &\delta_{\mathbf{k}\mathbf{k}'}\leftrightarrow(2\pi)^3\delta(\mathbf{k}-\mathbf{k}')\ . \end{aligned} \tag{5.3}$$

(2) The impurity atom is located at the origin. The operator $c^\dagger_{kM}$ creates a spherical-wave conduction state with wave vector $k=|\mathbf{k}|$ and total angular momentum M. Additional quantum numbers l and j (3 and $\frac{5}{2}$ in the case of Ce) are implicit. The spherical-wave normalization[27] is chosen to eliminate factors of 4π in final results:

$$\begin{aligned} &\langle\mathbf{r}\sigma|c^\dagger_{kM}|0\rangle=\sqrt{4\pi}i^l j_l(kr)\langle\sigma|m\rangle Y_{l,M-\sigma}(\hat{\mathbf{r}})\ ,\\ &\{c_{kM},c^\dagger_{k'M'}\}=(2\pi)^3\delta(k-k')\delta_{MM'}/4\pi k^2\ , \end{aligned} \tag{5.4}$$

where

$$\langle \sigma \mid M \rangle \equiv \langle l\tfrac{1}{2}\, M-\sigma\, \sigma \mid jM \rangle \ .$$

(The convention for Clebsch-Gordon coefficients and spherical harmonics is that of Messiah.[28]) In formal sums over spherical-wave states,

$$\sum_k \leftrightarrow \int_0^\infty dk\, 4\pi k^2/(2\pi)^3 \ , \qquad \delta_{kk'} \leftrightarrow (2\pi)^3 \delta(k-k')/4\pi k^2 \ . \tag{5.5}$$

The spherical-wave and plane-wave operators are related by

$$c^\dagger_{kM} = \sum_\sigma \int \frac{d\hat{\mathbf{k}}}{4\pi} \alpha_\sigma(M;\hat{\mathbf{k}}) c^\dagger_{\mathbf{k}\sigma} \ , \qquad \alpha_\sigma(M;\hat{\mathbf{k}}) = \sqrt{4\pi}\langle \sigma \mid M \rangle Y_{l,M-\sigma}(\hat{\mathbf{k}}) \ . \tag{5.6}$$

(3) The impurity Hilbert space contains only the empty state $\mid 0\rangle$ and singly occupied states $\mid M\rangle$. The eigenstate phases are chosen to make $V(k)$, the hybridization matrix element with band states, real valued.

VI. THE SINGLE-IMPURITY t MATRIX

The single-impurity t matrix is computed in two steps. First, $\hat{t}$ is expressed in terms of local operator averages; second, the local averages themselves are evaluated.

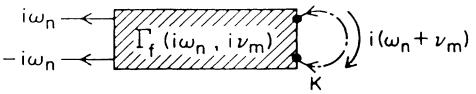

FIG. 11. Representation of the anomalous impurity Green's function $F_f(i\omega_n)$. Since only terms linear in the order parameter are retained, exactly one anomalous conduction propagator (denoted by the dash-dotted line) appears. The two large dots denote interaction vertices. The shaded rectangle Γ_f is a two-electron scattering vertex with factors of V removed.

A. Reduction of the t matrix

For convenience, we introduce the fully dressed normal and anomalous impurity Green's functions

$$G_f(MM';i\omega_n) = \int_0^\beta d\tau\, e^{i\omega_n\tau}[-\langle T_\tau F_M(\tau) F^\dagger_{M'}(0)\rangle] \ , \tag{6.1}$$

and

$$F_f(MM';i\omega_n) = \int_0^\beta d\tau\, e^{i\omega_n\tau}[-\langle T_\tau F_M(\tau) F_{M'}(0)\rangle] \ ,$$

with

$$F_M \equiv \mid 0\rangle\langle M \mid \ . \tag{6.2}$$

A perturbative expansion, or equation-of-motion approach, yields the following exact expression for the forward-scattering t matrix:

$$\hat{t}(\hat{\mathbf{k}};i\omega_n) = V^2 \begin{bmatrix} \alpha(M;\hat{\mathbf{k}}) G_f(MM';i\omega_n)\alpha^\dagger(M';\hat{\mathbf{k}}) & -\alpha(M;\hat{\mathbf{k}}) F_f(MM';i\omega_n)\alpha^T(M';-\hat{\mathbf{k}}) \\ \alpha^*(M;-\hat{\mathbf{k}}) F^*_f(MM';i\omega_n)\alpha^\dagger(M';\hat{\mathbf{k}}) & -\alpha^*(M;\hat{\mathbf{k}}) G^*_f(MM';i\omega_n)\alpha^T(M';-\hat{\mathbf{k}}) \end{bmatrix} \ . \tag{6.3}$$

Here $\alpha(M;\hat{\mathbf{k}})$ denotes a two-element column vector with entries α_σ [see Eq. (5.6)]; each element in (6.3) is a 2×2 spin matrix. Sums over M and M' are implied. The hybridization V is evaluated at the Fermi surface. Use has been made of the identity

$$\int_0^\beta d\tau\, e^{i\omega_n\tau}\langle T_\tau A^\dagger(\tau) B^\dagger(0)\rangle = -\int_0^\beta d\tau\, e^{i\omega_n\tau}\langle T_\tau A(\tau) B(0)\rangle^* \ . \tag{6.4}$$

The next step in the simplification of $\hat{t}$ involves performing the sums over the magnetic quantum numbers M and M' in (6.3). For the terms involving G_f, this is relatively simply since

$$G_f(MM';i\omega_n) = G_f(i\omega_n)\delta_{MM'} \tag{6.5}$$

by rotational invariance. In the case of the anomalous propagator, three points should be noted. First, only terms linear in the gap function $[\Delta(\hat{\mathbf{k}})]_{\sigma\sigma'}$ need be retained to deduce T_c. Second, since s-wave pairing with an isotropic gap is assumed for simplicity,

$$[\Delta(\hat{\mathbf{k}})]_{\sigma\sigma'} = \begin{bmatrix} 0 & \Delta \\ -\Delta & 0 \end{bmatrix} = \Delta(-1)^{1/2-\sigma}\delta_{\sigma,-\sigma'} \ . \tag{6.6}$$

Third, to linear order in Δ, F_f may be represented by Fig. 11; the vertex $\Gamma_f(i\omega_n, i\nu_m)$ is evaluated in the next section. Computing Fig. 11 gives (see Appendix C)

$$F_f(MM';i\omega_n) = \frac{1}{\beta}\sum_m K(MM';i(\omega_n+\nu_m))\Gamma_f(i\omega_n, i\nu_m)$$

with

$$K(MM';i(\omega_n+\nu_m)) = N(0)V^2 \int \frac{d\hat{\mathbf{k}}}{4\pi} \alpha^\dagger(M;\hat{\mathbf{k}}) \hat{g}^{12}_0(\hat{\mathbf{k}};i(\omega_n+\nu_m))\alpha^*(M';-\hat{\mathbf{k}}) \tag{6.7}$$

and

$$\hat{g}_0^{12}(\hat{\mathbf{k}};i\omega_n)=\frac{\pi[\Delta(\hat{\mathbf{k}})]_{\sigma\sigma'}}{|\omega_n|} .$$

[See Eq. (A2).] Substituting (6.6) for $[\Delta(\hat{\mathbf{k}})]_{\sigma\sigma'}$ and (5.6) for $\alpha_\sigma(M;\hat{\mathbf{k}})$ yields

$$K(MM';i(\omega_n+\nu_m))=(\Gamma/\pi)\frac{\pi\Delta}{|\omega_n+\nu_m|}\sum_{\sigma,\sigma'}\int\frac{d\hat{\mathbf{k}}}{4\pi}Y^*_{l,M-\sigma}(\hat{\mathbf{k}})Y^*_{l,M'-\sigma'}(-\hat{\mathbf{k}})(-1)^{1/2-\sigma}\delta_{\sigma,-\sigma'}\langle\sigma\,|\,M\rangle\langle\sigma'\,|\,M'\rangle$$

$$=\frac{\Gamma\Delta}{|\omega_n+\nu_m|}\delta_{M,-M'}(-1)^{j+M} . \tag{6.8}$$

To summarize,

$$F_f(MM';i\omega_n)=\delta_{M,-M'}(-1)^{j+M}F_f(i\omega_n) ,$$
$$F_f(i\omega_n)=\Gamma\Delta\frac{1}{\beta}\sum_m\frac{\Gamma_f(i\omega_n,i\nu_m)}{|\omega_n+\nu_m|} . \tag{6.9}$$

Expressions (6.5) and (6.9) for G_f and F_f lead to the following sums when inserted in (6.3):

$$\sum_M\alpha_\sigma(M;\hat{\mathbf{k}})\alpha^\dagger_{\sigma'}(M;\hat{\mathbf{k}})=\tfrac{1}{2}(2j+1)\delta_{\sigma\sigma'}$$

and

$$-\sum_M\alpha_\sigma(M;\hat{\mathbf{k}})\alpha^T_{\sigma'}(-M;-\hat{\mathbf{k}})(-1)^{j+M}=\tfrac{1}{2}(2j+1)(-1)^{1/2-\sigma}\delta_{\sigma,-\sigma'} . \tag{6.10}$$

Additional terms in (6.3) can be deduced from (6.10) by complex conjugating and letting $\hat{\mathbf{k}}\to-\hat{\mathbf{k}}$. [The evaluation of (6.10) proceeds by writing out α explicitly as in (6.8).]

Equation (6.3) may now be simplified to

$$\hat{t}(\hat{\mathbf{k}};i\omega_n)=\frac{2j+1}{2}V^2\begin{bmatrix}G_f(i\omega_n)\mathbb{1} & F_f(i\omega_n)(i\sigma_2)\\ F_f(i\omega_n)(-i\sigma_2) & -G_f^*(i\omega_n)\mathbb{1}\end{bmatrix} ,$$
$$F_f(i\omega_n)=\Gamma\Delta\frac{1}{\beta}\sum_m\frac{\Gamma_f(i\omega_n,i\nu_m)}{|\omega_n+\nu_m|} . \tag{6.11a}$$

The scattering amplitudes displayed in our initial discussion of results (cf. Figs. 2 and 3 and 5–8) may now be defined more precisely:

$$T_1(\omega)=\frac{2j+1}{2}V^2G_f(\omega) ,$$
$$T_2^{\text{elast}}(\omega)=\frac{2j+1}{2}V^4T\Gamma_f(\omega,-\omega;0) , \tag{6.11b}$$
$$T_2^{\text{SF}}(\omega)=\frac{2j+1}{2}V^4T\Gamma_f(\omega,-\omega;-2\omega) .$$

Finally, using Eq. (4.10) for $(-dT_c/dC)\,|_{C=0}$, we write

$$(-dT_c/dC)\,|_{C=0}=-\frac{2j+1}{2}\pi V^2T_{c0}^2\sum_n\left[\frac{\operatorname{Im}G_f(i\omega_n)}{\omega_n^2}\operatorname{sgn}\omega_n+\frac{F_f(i\omega_n)}{\Delta|\omega_n|}\right] , \tag{6.12}$$

with $\omega_n=(2n+1)\pi T_{c0}$. The next section is devoted to evaluating $G_f(i\omega_n)$ and $F_f(i\omega_n)$.

B. Evaluation of propagators G_f and F_f

Consider the impurity Green's function G_f of Eq. (6.1). To linear order in Δ, only normal-state contributions to G_f are allowed. G_f may be represented by the general technique for treating systems with strong local correlations;[29] this method is considerably more concise and elegant than the alternate pseudo-Hamiltonian approach.[30] We summarize in Table II the rules for evaluating general contributions to G_f; a step-by-step example is illustrated in Fig. 12. These rules are derived in detail in Appendix C. It is possible to reformulate per-

turbation theory in the hybridization $V(k)$ as an expansion in $1/N$, where $N=2j+1$ is the degeneracy of the f impurity. Diagrams may be classified in powers of $1/N$, provided the quantity $NV^2(k)$ is treated as $O(1)$. Alternatively, the expansion may be generated by the replacement

$$V(k)=\tilde{V}(k)/\sqrt{N} \ . \tag{6.13}$$

This $1/N$ expansion formally improves in accuracy with increasing degeneracy. Neglecting crystal-field effects, the spin-orbit ground state of Ce is sixfold degenerate; one expects the $1/N$ expansion to yield a useful approximation scheme in such a case.

It has been demonstrated that all contributions to G_f of $O(1)$ and $O(1/N)$, as well as an extensive set of higher-order contributions, may be summed by computing the diagram in Fig. 13:

$$G_f(MM';i\omega_n)\approx\delta_{MM'}\frac{1}{Z_f}\int_\Gamma\frac{dz}{2\pi i}e^{-\beta z}G_0(z)G_M(z+i\omega_n) , \tag{6.14}$$

$$Z_f=\int_\Gamma\frac{dz}{2\pi i}e^{-\beta z}[G_0(z)+NG_M(z)] \ .$$

The double lines denote G_0 and G_M, dressed propagators for the empty and occupied states computed using the self-energies shown in Fig. 14:

$$\begin{aligned} G_0(z)&=\frac{1}{z-\Sigma_0(z)} \ , \\ G_M(z)&=\frac{1}{z-\varepsilon_f-\Sigma_M(z)} \ , \\ \Sigma_0(z)&=NV^2\sum_k f_k G_M(z+\varepsilon_k) \ , \\ \Sigma_M(z)&=V^2\sum_k(1-f_k)G_0(z-\varepsilon_k) \ . \end{aligned} \tag{6.15}$$

The reduction of the summation to solution of a closed set of coupled equations is possible since vertex corrections to G_f, G_0, and G_M enter only at $O(1/N^2)$. The preceding scheme has been called the "noncrossing approximation," or NCA, since it sums all contributions to G_0 and G_M arising from diagrams with noncrossing conduction electron lines.[2]

It is convenient to introduce spectral densities associated with the propagators in Eqs. (6.14) and (6.15):

$$\begin{aligned} \rho_0(\epsilon)&=-\frac{1}{\pi}\,\mathrm{Im}\,G_0(\epsilon+i0^+) \ , \\ \rho_M(\epsilon)&=-\frac{1}{\pi}\,\mathrm{Im}\,G_M(\epsilon+i0^+) \ , \\ \rho_f(\epsilon)&=-\frac{1}{\pi}\,\mathrm{Im}\,G_f(\epsilon+i0^+) \ . \end{aligned} \tag{6.16}$$

From Eq. (6.15), it follows that

$$\rho_f(\omega)=\frac{1}{Z_f}(1+e^{-\beta\omega})\int_{-\infty}^{\infty}d\epsilon\, e^{-\beta\epsilon}\rho_0(\epsilon)\rho_M(\epsilon+\omega) \ , \tag{6.17}$$

with

$$Z_f=\int_{-\infty}^{\infty}d\epsilon\, e^{-\beta\epsilon}[\rho_0(\epsilon)+N\rho_M(\epsilon)] \ .$$

Consider now the two-particle vertex Γ_f introduced in Eq. (6.7). It is demonstrated in Appendix C that this vertex may be calculated using the rules in Table III; an example is shown in Fig. 15.

The simplest contribution to Γ_f has the diagrammatic form shown in Fig. 16(a):

$$\Gamma_f^0(i\omega_n,i\nu_m)=\frac{1}{Z_f}\int_\Gamma\frac{dz}{2\pi i}e^{-\beta z}\frac{1}{z-\varepsilon_f}\frac{1}{z+i(\omega_n+\nu_m)} \times\frac{1}{z+i(2\omega_n+\nu_m)-\varepsilon_f}\frac{1}{z+i\omega_n} \ , \tag{6.18}$$

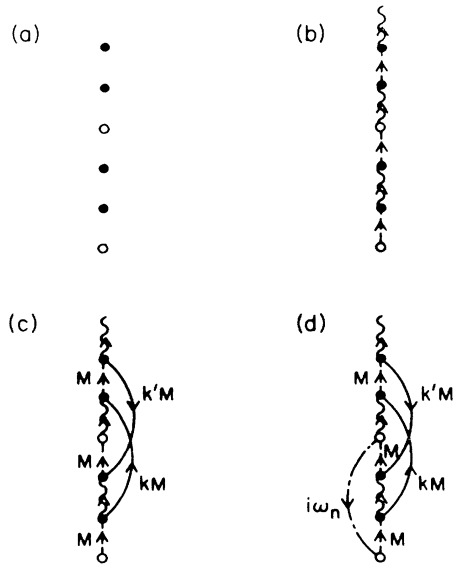

FIG. 12. Illustration of rules for constructing the normal impurity Green's function G_f. (a) Vertices. Solid circles denote interaction vertices, and open circles the operators F_M and $F_M^\dagger$. An even number of interaction vertices is interposed between the creation and destruction operator. (b) Addition of f configuration lines. Wavy lines represent the empty state, and dashed lines the occupied states. (c) Addition of conduction electrons (solid lines) and assignment of quantum numbers. (d) Addition of an "external line." The external line carries Fermi frequency $i\omega_n$ between f destruction and creation operator. The complete contribution of this diagram to G_f is

$$(-1)\frac{1}{N^2}(NV^2)^2\frac{1}{Z_f}\int_\Gamma\frac{dz}{2\pi i}e^{-\beta z}\frac{1}{z}\sum_{kk'}(1-f_k)f_{k'} \times\frac{1}{z+\varepsilon_{k'}-\varepsilon_f}\frac{1}{z-\varepsilon_k+\varepsilon_{k'}}\frac{1}{z+i\omega_n-\varepsilon_k+\varepsilon_{k'}-\varepsilon_f} \times\frac{1}{z+i\omega_n-\varepsilon_k}\frac{1}{z+i\omega_n-\varepsilon_f} \ ,$$

where Γ encircles all singularities of the integrand in a counterclockwise fashion. The minus sign arises from the single conduction line crossing.

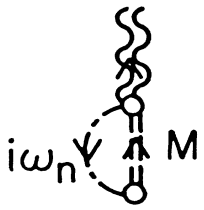

FIG. 13. Expression for G_f in the self-consistent large-degeneracy expansion, or "noncrossing approximation." The double wavy and double dashed lines represent dressed propagators for the empty and occupied states, computed using the self-energies of Fig. 14.

where the contour Γ encircles all singularities of the integrand in a counterclockwise fashion. The empty and occupied state lines may be dressed with self-energy insertions, as discussed previously, and vertex corrections are also a possibility [see Figs. 16(b)–16(d)]. As in the case of G_f, the leading and next-leading contributions to Γ_f in a formal $1/N$ expansion (as well as the extensive class of higher-order noncrossing contributions) may be summed by dressing G_0 and G_M with the self-energies computed in Eq. (6.15). The resulting diagram is indicated in Fig. 16(e); the expression for Γ_f is the same as Eq. (6.18) with

$$\frac{1}{z}\rightarrow G_0(z), \quad \frac{1}{z-\varepsilon_f}\rightarrow G_M(z) \; . \tag{6.19}$$

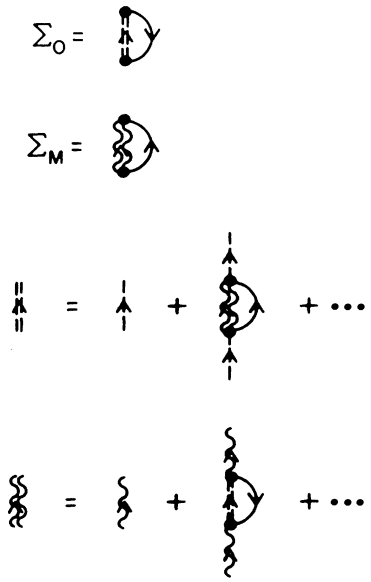

FIG. 14. Self-consistent approximation for the empty- and occupied-state self-energies.

Due to the presence of the additional factor

$$\Gamma=\pi N(0)V^2=\frac{1}{N}(N\Gamma) \; , \tag{6.20}$$

F_f [Eq. (6.2)] is formally smaller than G_f [Eq. (6.1)] by a

TABLE II. Diagrammatic rules for evaluating $G_f(i\omega_n)$. We list below rules for evaluating the normal-state f Green's function $G_f(i\omega_n)$.

To compute a general contribution to $G_f(i\omega_n)$ of $O(V^{2n})$, $n \geq 0$.

(a) Set down $2n+2$ vertices (solid circles) in a vertical line. Beginning at the bottom with a dashed line, connect the vertices with alternating dashed and wavy lines (all ascending), finally leaving the top vertex on a wavy line. (A total of $2n+2$ lines now appear.)

(b) Counting from the bottom, convert the first vertex to an open circle (to represent the operator $F_M^\dagger$); convert an even-numbered vertex to an open circle (to represent the operator F_M).

(c) Always working to the right of the vertical line, connect the remaining $2n$ vertices with solid lines in all possible ways which maintain the direction of the dashed line at each vertex.

(d) Working on the left-hand side of the diagram, connect the open circles with a dashed-dotted "external line," carrying energy $i\omega_n$ from top to bottom.

(e) Assign quantum numbers $kM(M)$ to solid lines (dashed lines), conserving angular momentum at each vertex.

(f) Assign to ascending band lines a factor $1-f_{kM}$ and to descending band lines a factor f_{kM}, with f the Fermi function.

(g) Draw a perpendicular to each local configuration line, and assign to it an energy denominator $(z-E_\alpha)^{-1}$, where E_α is found by adding the energies of ascending lines intersected by the perpendicular and subtracting the energies of descending lines intersected.

(h) Multiply the product of energy denominators and Fermi factors by $V^{2n}(-1)^c$. Here c is the number of line crossings on the right-hand side of the diagram. Sum on conduction momenta and internal angular momenta.

(i) Compute the contour integral $(1/Z_f)\int_\Gamma (dz/2\pi i)e^{-\beta z}R(z)$, where R is the result of the preceding operations, Z_f is the system partition function, and Γ encircles all singularities of R in a counterclockwise fashion.

factor of $1/N$. Hence, to compute the shift in T_c with formal errors of $O(1/N)$ in the impurity Green's functions G_f and F_f, G_0 and G_M need only be dressed to terms of $O(1)$ in F_f. This requires only the calculation of the empty-state self-energy shown in Fig. 16(f). (Corresponding simplifications may be made in the evaluation of G_f.) Note, however, that the computational effort required for the evaluation of F_f in this approach is not significantly reduced over that in the NCA. As shown in Appendix D, the limiting step in the evaluation of F_f within the NCA is the computation of a set of triple spectral integrals. Such integrals cannot be completely eliminated by leaving the occupied-state lines bare.

Expressions have now been derived for G_f and Γ_f. It remains to reduce the frequency sums over dressed propagators in Eq. (6.12) to spectral integrals for numerical evaluation. The full summations are performed in Appendix D. The resulting expression for the two-particle contribution involves highly singular triple spectral integrals, which have not been evaluated numerically. Instead, a simple approximation for this contribution has been introduced. In this approximation, only elastic and elastic spin-flip processes are retained (see Fig. 17). Since these are exactly the processes which enter the original AG calculation,[14] this may be termed an "energy-dependent AG approximation." The equations for the two-particle contribution below assume this approximation. One finds

$$(-dT_c/dC)\,|_{C=0}=(-dT_c/dC)_1+(-dT_c/dC)_2\ , \tag{6.21a}$$

where

$$N(0)(-dT_c/dC)_1=\tfrac{1}{2}N\Gamma\int_{-\infty}^{\infty}d\omega\,\rho_f(\omega)R_1(\omega) \tag{6.21b}$$

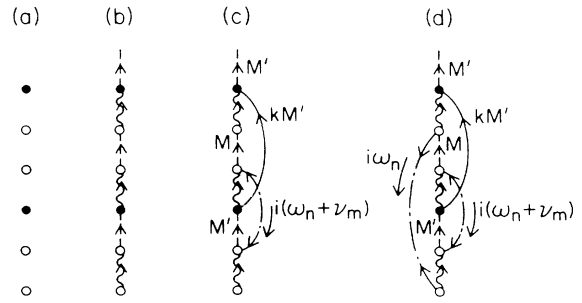

FIG. 15. Illustration of the rules for computing the two-particle scattering vertex Γ_f. (a) Vertices. Solid circles denote interaction vertices; open circles denote the operators F_M and $F_{M'}^{\dagger}$ and the points of attachment for the anomalous conduction line K (cf. Fig. 11). Counting from the bottom, two open circles must appear in even positions and two in odd positions. (b) Addition of f configuration lines. (c) Addition of conduction lines and quantum numbers. Interaction vertices are connected by normal (solid) lines, and the open circles in even positions by an anomalous (dash-dotted) line. (d) Addition of an "external line." The external line carries frequency $i\omega_n$ between the remaining open circles. The total contribution of this diagram to Γ_f is

$$(-1)^2\frac{1}{N}(NV^2)\frac{1}{Z_f}\int_\Gamma\frac{dz}{2\pi i}e^{-\beta z}\frac{1}{z-\varepsilon_f}$$
$$\times\sum_k\frac{(1-f_k)}{z-\varepsilon_k}\frac{1}{z+i\omega_n-\varepsilon_k-\varepsilon_f}\frac{1}{z+i(2\omega_n+i\nu_m)-\varepsilon_k}$$
$$\times\frac{1}{z+i(2\omega_n+\nu_m)-\varepsilon_f}\frac{1}{z+i\omega_n}\ .$$

The sign is $(-1)^{c+g}$, with $c=g=1$.

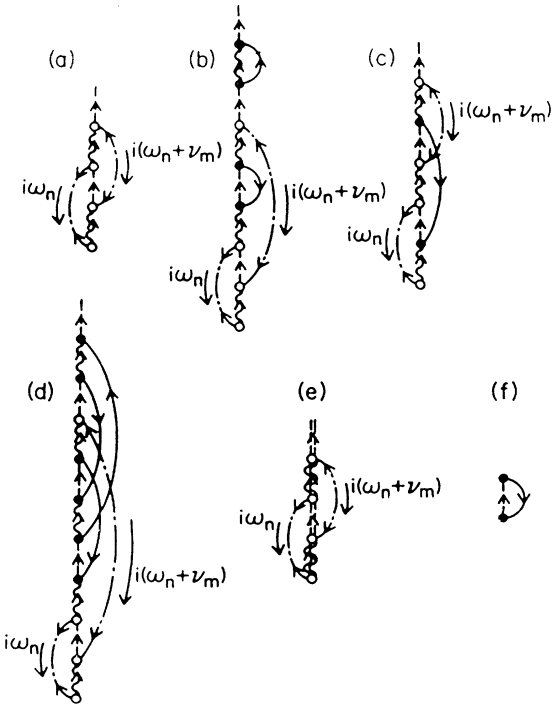

FIG. 16. Diagrammatic contributions to Γ_f. (a) Simplest diagrammatic contribution to Γ_f. (b) A contribution to Γ_f with empty- and occupied-state self-energy insertions. (c) and (d) Vertex corrections to Γ_f. (e) Representation of Γ_f within the self-consistent approach. The double wavy and double dashed lines incorporate the self-energies of Fig. 14. (f) Lowest-order empty-state self-energy.

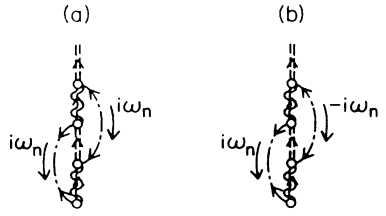

FIG. 17. Diagrammatic representation of the elastic and elastic spin-flip parts of the vertex Γ_f. (a) Elastic. (b) Elastic spin flip.

with

$$R_1(\omega)=-\frac{T}{\pi\omega^2}\left[\psi(\tfrac{1}{2})-\mathrm{Re}\,\psi\left[\frac{1}{2}+\frac{i\omega}{2\pi T}\right]\right],$$

$$\rho_f(\omega=\frac{1}{Z_f}(1+e^{-\beta\omega})\int_{-\infty}^{\infty}d\epsilon\, e^{-\beta\epsilon}\rho_0(\epsilon)\rho_M(\epsilon+\omega),$$

$$Z_f=\int_{-\infty}^{\infty}d\epsilon\, e^{-\beta\epsilon}[\rho_0(\epsilon)+N\rho_M(\epsilon)], \tag{6.21c}$$

and

$$N(0)(-dT_c/dC)_2=\tfrac{1}{2}N\Gamma^2\int_{-\infty}^{\infty}d\omega[\sigma_f(\omega)-(M\leftrightarrow 0)]R_2(\omega) \tag{6.21d}$$

with

$$R_2(\omega)=\frac{T}{4\omega}\left[1-\frac{2T}{\omega}\tanh\left[\frac{\omega}{2T}\right]\right],$$

$$\sigma_f(\omega)=\frac{1}{Z_f}\int_{-\infty}^{\infty}d\epsilon\, V(\epsilon;\omega), \tag{6.21e}$$

$$V(\epsilon;\omega)=4\cosh(\omega/2T)e^{-\beta\epsilon}\,\mathrm{Re}\,G_0(\epsilon)\rho_0(\epsilon)[e^{\beta\omega/2}\rho_M(\epsilon-\omega)\,\mathrm{Re}\,G_M(\epsilon+\omega)-e^{-\beta\omega/2}\rho_M(\epsilon+\omega)\,\mathrm{Re}\,G_M(\epsilon-\omega)]$$
$$+2\sinh(\omega/T)e^{-\beta\epsilon}[\,\mathrm{Re}^2G_0(\epsilon)-\pi^2\rho_0^2(\epsilon)]\rho_M(\epsilon+\omega)\rho_M(\epsilon-\omega).$$

TABLE III. Diagrammatic rules for evaluating $\Gamma_f(i\omega_n,i\nu_m)$. We list below rules for evaluating the two-electron scattering vertex $\Gamma_f(i\omega_n,i\nu_m)$, which appears in the expression for T_c depression [Eq. (6.11)]. These rules follow simply from those derived from the anomalous f Green's function in Appendix C.

To compute a general contribution to $\Gamma_f(i\omega_n,i\nu_m)$ of $O(V^{2n})$, $n\geq 0$.

(a) Set down $2n+4$ vertices (solid circles) in a vertical line. Beginning at the bottom with a wavy line, connect the vertices with alternating wavy and dashed lines (all ascending), finally leaving the highest vertex on a dashed line. (A total of $2n+4$ lines now appear.)

(b) Convert four vertices to open circles, representing the points at which incoming and outgoing external conduction lines may be attached: counting from the bottom, convert the first vertex and one other odd-numbered vertex (possible points of attachment for outgoing external lines), and two even-numbered vertices (possible points of attachment for incoming external lines).

(c) Always working to the right of the vertical line, connect the remaining $2n$ vertices with solid lines in all possible ways which maintain the direction of the dashed line at each vertex.

(d) Working on the left-hand side of the diagram, connect the open circles at odd-numbered points with a dashed-dotted "external line." This line carries angular momentum M into the top circle, M' into the bottom circle, and "energy" $i\omega_n$ from top to bottom.

(e) Working on the right-hand side of the diagram, connect the remaining open circles (at even-numbered vertices) with a dashed-dotted "external line," carrying "energy" $i(\omega_n+\nu_m)$ from top to bottom. (This line carries the angular momenta M and M' out of the diagram.)

(f) Assign quantum numbers kM (M) to solid lines (dashed lines), conserving angular momentum at each vertex.

(g) Assign to ascending band lines a factor $1-f_{kM}$ and to descending band lines a factor f_{kM}, with f the Fermi function.

(h) Draw a perpendicular to each local configuration line, and assign to it an energy denominator $(z-E_\alpha)^{-1}$, where E_α is found by adding the energies of ascending lines intersected by the perpendicular and subtracting the energies of descending lines intersected.

(i) Multiply the product of energy denominators and Fermi factors by $V^{2n}(-1)^{c+g}$. Here, c is the number of line crossings on the right-hand side of the diagram (including the external line); g is zero if a continuous path of dashed and solid lines can be traced between the lower end point of the dashed-dotted line on the right and the upper end point of the dash-dotted line on the left; and 1 otherwise. Sum on conduction momenta and internal angular momenta.

(j) Compute the contour integral $(1/Z_f)\int_\Gamma(dz/2\pi i)e^{-\beta z}R(z)$, where R is the result of the preceding operations, Z_f is the system partition function, and Γ encircles all singularities of R in a counterclockwise fashion.

All functions are evaluated at $T=T_{c0}$. The notation $(M\leftrightarrow 0)$ indicates the interchange of subscripts M and 0 in the expression defining $\sigma_f(\omega)$, i.e., in $V(\epsilon;\omega)$. Note that $\sigma_f(\omega)$ and $R_2(\omega)$ are both manifestly odd in ω; σ_f arises from elastic scattering, and $\sigma_f \mid_{M\leftrightarrow 0}$ from elastic spin-flip scattering.

VII. NUMERICAL RESULTS

Numerical studies of T_c depression in the extremely dilute limit have been carried out using the energy-dependent AG approximation summarized in Eqs. (6.21). This approximation avoids evaluation of the triple spectral integrals which necessarily emerge when inelastic processes are included. The approximation is poorest for large values of T_0/T_{c0}; a simple continuity argument suggests that $\Gamma_f(i\omega_n,i\nu_m)\approx\Gamma_f(i\omega_n,0)$ for small $\nu_m=2\pi m T_{c0}$. In this limit, inelastic processes with energy transfer up to $\sim T_0$ are expected to be important for correctly reproducing the crossover from pair-breaking to pair-weakening behavior. On the other hand, we expect the approximation to be adequate for smaller values of T_0/T_{c0}; in particular, the location and magnitude of the peak depression rate should be little affected by the omission of inelastic processes.

Results for initial T_c depression are plotted in Fig. 10 as a function of T_0/T_{c0}, where T_0 is the peak position of $\rho_f(\omega;T\rightarrow 0)$, the f density of states at zero temperature. The curves were generated using three choices of conduction–f-electron hybridization Γ. In each case, a Lorentzian conduction density of states with half-width D was assumed. For each choice of hybridization (and hence of T_0), the value of T_{c0} was varied over a range of approximately three decades. Parameter choices are summarized in Table I. The value of T_0 may be deduced within a factor of order unity by simple scaling arguments (see Ref. 1); the detailed band shape is expected to provide a nonuniversal prefactor in such calculations.

The initial depression of T_c assumes a scaling form (Fig. 10) in the parameter range studied, i.e., it is determined solely by the ratio of the Kondo scale T_0 and the transition temperature of the pure system T_{c0}. Such scaling behavior has been derived previously by Müller-Hartmann and Zittartz. Within the present treatment, scaling follows from the nearly universal form of the low-temperature one- and two-electron t matrices T_1 and T_2 for $\omega,T\ll|\varepsilon_f|$, Γ, and D (see Figs. 3, 7, and 8). The scaling behavior of T_1 and the f-electron density of states ρ_f imply low-temperature scaling for normal-state properties as well. The transport and thermodynamic properties of Ce systems[1] have been calculated for the parameter sets of Table I.

The pair-breaking effect shown in Fig. 10 is anomalously large for $T_0/T_{c0}\approx 1$; maximal depression occurs for $T_0\approx 5T_{c0}$. A similar result emerged in the Kondo Hamiltonian studies of MHZ (Ref. 18) and MIN (Ref. 22). The source of strong pair breaking and T_c depression in all three calculations is the decreased lifetime of superconducting pairs due to resonant scattering near the Fermi surface. For comparison, a representative depression rate for magnetic impurities in the absence of the Kondo effect (i.e., for $T_0\rightarrow 0$) is indicated by the small arrow in Fig. 10. This rate was computed for the first parameter set in Table I using the AG expression of Eq. (B19).

The giant depression in the presence of the Kondo effect is due to the Kondo-Abrikosov-Suhl resonance in the f-electron density of states. The single-electron scattering rate for the conduction band is proportional to this local density of states. Since each impurity site has magnetic character (before Kondo quenching is complete), singlet-paired electrons do not scatter from impurities "in tandem" (as they would in a time-reversal symmetric system.) Thus, for $T_0/T_{c0}\approx 1$, the Kondo resonance manifests itself in strong Cooper pair breaking as well as in strong single-electron scattering.

The prediction of $(-dT_c/dC)\mid_{C=0}$ for a specific system requires three parameters: T_{c0}, $N(0)$, and T_0. T_0 may be measured in the normal state, e.g., by fitting to the resistivity curve of Ref. 1. The density of states may also be deduced from normal-state measurements, or from band-structure calculations. A possible system for comparison of theory and experiment is the series of alloys (La,Th)Ce;[9] in this system, the conduction–f-electron hybridization may be tuned continuously by varying the La and Th concentrations. Previous theories (MHZ and MIN) have produced predictions for the functional form of the specific heat discontinuity $\Delta C/C$, which may be measured along with T_c. The correlation of values for these two quantities provides a theoretical consistency test. We have not attempted to evaluate $\Delta C/C$: such a calculation requires the evaluation of the free energy below T_c to terms of $O(\Delta^3)$. For this reason, comparison of our theory with experiment requires correlation with some normal-state property, such as resistivity or susceptibility. Sufficiently precise measurements of $(-dT_c/dC)\mid_{C=0}$ and normal-state properties in a single system do not presently exist, to our knowledge.

VIII. CONCLUSIONS

The formalism developed in the preceding sections allows the treatment of superconducting T_c depression by magnetic impurities within the same framework used to investigate normal-state properties.[1] The good agreement between thermodynamic results in the self-consistent large-degeneracy expansion and in Bethe-ansatz studies provides a measure of the expected accuracy of dynamic results such as the resistivity, dynamic susceptibility, and shift in T_c. A key approximation in the numerical evaluation of $(-dT_c/dC)\mid_{C=0}$ reported here is the neglect of inelastic contributions to the two-particle scattering vertex; we do not expect this omission to significantly alter the position and magnitude of the peak depression or the form of $(-dT_c/dC)\mid_{C=0}$ for values of $T_0/T_{c0}\leq 1$.

In the integral valent limit, the initial depression is largest when T_{c0} is smaller than T_0 by a factor of ≈ 5 (see Fig. 10). This result is in qualitative agreement with the treatment of Kondo impurities by MHZ (Ref. 18)

and MIN (Ref. 22). The maximum depression is anomalously large in comparison with that of AG theory[14] and is in good agreement with the prediction of MHZ theory.

Future work may concentrate on the form of T_c for finite impurity concentrations. A detailed numerical study is required in order to discuss the possible occurrence of reentrant superconductivity.

ACKNOWLEDGMENTS

We thank J. W. Wilkins and D. L. Cox for their continuous help and suggestions. We also thank E. Müller-Hartmann for useful conversations and correspondence. One of us (N.E.B.) was partially supported by the National Science Foundation. Another of us (G.E.Z.) was supported by the Max Kade Foundation. This work was supported in part by the National Science Foundation through Grant No. DMR-83-14764.

APPENDIX A: SOLUTION OF THE DILUTE IMPURITY EILENBERGER EQUATION

In this appendix the dilute impurity Eilenberger equation[25] (4.6) is solved and the general form for $(-dT_c/dC)\,|_{C=0}$ cited in Eq. (4.8) is derived. We assume an isotropic singlet order parameter, and without loss set the quasiparticle renormalization constant $a=1$. We assume in addition the forward-scattering t matrix is isotropic (as it is for the Hamiltonian of Sec. V). Then the form for $\hat{t}$ in Eq. (4.7) follows, i.e., $\hat{t}$ may be expressed in terms of the particle-hole diagonal and off-diagonal scattering amplitudes, $t_1(i\omega_n)$ and $t_2(i\omega_n)$. Let

$$\hat{g}(\hat{\mathbf{k}};i\omega_n)=g_1(i\omega_n)\hat{\tau}_3+g_2(i\omega_n)(i\sigma_2)\hat{\tau}_1 \tag{A1}$$

and recall[25] that

$$\hat{g}_0(i\omega_n)=-i\pi\,\mathrm{sgn}\,\omega_n\hat{\tau}_3+\frac{\pi\Delta}{|\omega_n|}(i\sigma_2)\hat{\tau}_1\ . \tag{A2}$$

The commutator equation (4.6) may be rewritten

$$i\omega_n g_2(i\omega_n)+\Delta g_1(i\omega_n) =C\Delta\left[i\,\mathrm{Im}t_1(i\omega_n)\frac{\pi}{|\omega_n|}+(i\pi\,\mathrm{sgn}\,\omega_n)\frac{t_2(i\omega_n)}{\Delta}\right]. \tag{A3}$$

The normalization condition is simply

$$g_1^2(i\omega_n)-g_2^2(i\omega_n)=g_1^2(i\omega_n)+O(\Delta^2)=-\pi^2\ , \tag{A4}$$

giving to linear order in Δ,

$$g_1(i\omega_n)=-i\pi\,\mathrm{sgn}\omega_n\ . \tag{A5}$$

Solving Eq. (A3),

$$g_2(i\omega_n)=\frac{\pi\Delta}{|\omega_n|}\left[1+\frac{C\,\mathrm{Im}\,t_1(i\omega_n)(\mathrm{sgn}\,\omega_n)}{|\omega_n|}+\frac{Ct_2(i\omega_n)}{\Delta}\right]. \tag{A6}$$

The linearized self-consistency equation is then

$$\Delta=\lambda T_c\sum_n{}'\,g_2(i\omega_n)\ , \tag{A7a}$$

i.e.,

$$1=\lambda T_c\sum_n{}'\frac{\pi}{|\omega_n|}\left[1+\frac{\mathrm{sgn}\,\omega_n}{|\omega_n|}C\,\mathrm{Im}\,t_1(i\omega_n)+\frac{Ct_2(i\omega_n)}{\Delta}\right]\Bigg|_{\Delta=0}. \tag{A7b}$$

Here λ is the dimensionless BCS coupling constant, and the prime implies a high-frequency cutoff on the order of the Debye temperature.

Noting that

$$T_c\sum_n{}'\frac{\pi}{|\omega_n|}-\lambda^{-1}=\ln(T_{c0}/T_c)\approx\frac{T_{c0}-T_c}{T_{c0}}\ , \tag{A8}$$

one finds

$$(-dT_c/dC)\,|_{C=0}=-\pi T_{c0}^2\sum_n\left[\frac{\mathrm{sgn}\,\omega_n}{\omega_n^2}\,\mathrm{Im}\,t_1(i\omega_n)+\frac{\Delta^{-1}t_2(i\omega_n)}{|\omega_n|}\right]\Bigg|_{\Delta=0}. \tag{A9}$$

APPENDIX B: RELATION TO ABRIKOSOV-GOR'KOV THEORY

While the approach discussed in the text is well suited for studies of T_c depression in the Kondo regime, it may also be used to derive the generalization of conventional AG theory[14] for the orbitally degenerate Anderson[4] or Coqblin-Schrieffer[27] models. This provides an expression for $(-dT_c/dC)\,|_{C=0}$ to second order in Γ/ε_f valid in the limit $T_0/T_{c0}\to 0$.

The Anderson model for magnetic impurities was introduced in Eq. (5.1):

$$H_A=H_{\mathrm{band}}+H_f+H_{\mathrm{mix}}\ . \tag{B1}$$

For an impurity level far below the Fermi surface ($\varepsilon_f\ll 0$), this Hamiltonian may be reduced by a canonical transformation[6] to the Coqblin-Schrieffer form[27]

$$H_{\mathrm{CS}}=H_{\mathrm{band}}-\sum_{k,k',M,M'}J_{kk'}c_{k'M'}^{\dagger}c_{kM}\,|\,M\rangle\langle M'\,|\ ,$$

where

$$J_{kk'}=\frac{V(k)V(k')U}{\varepsilon_f(\varepsilon_f+U)}\ , \tag{B2}$$

and all other symbols are as previously defined. H_{CS} acts within the space of states for which the impurity occupancy is unity.

The Coqblin-Schrieffer (CS) Hamiltonian describes combined spin and orbital exchange scattering and

reduces to the spin-$\frac{1}{2}$ Kondo Hamiltonian when $j=\frac{1}{2}$, $l=0$. In the limit $U\to\infty$,

$$J_{kk'}=V(k)V(k')/\varepsilon_f<0\ . \tag{B3}$$

For simplicity, the approximation

$$\begin{aligned} &V(k)=V=\text{ const}\ , \\ &J_{kk'}=J=\text{ const} \end{aligned} \tag{B4}$$

is employed below.

The results of Abrikosov and Gor'kov for the spin-$\frac{1}{2}$ Kondo model may be readily generalized to the Coqblin-Schrieffer model; a possible calculational approach utilizes a variation of Abrikosov's projection scheme.[31] The second Born approximation for T_c depression is instead derived below within the infinite-U Anderson model in the limit

$$\begin{aligned} &\varepsilon_f\to-\infty\ , \\ &V\to\infty\ , \\ &N(0)V^2/\varepsilon_f=N(0)J=\text{ const}\ll 1\ . \end{aligned} \tag{B5}$$

The analysis need not be restricted to low impurity concentrations in this case.

As in Sec. IV, the calculation consists of computing the quasiclassical Green's function $\hat{g}(\hat{\mathbf{k}};i\omega_n)$ of the superconductor in the presence of magnetic impurities, then applying the self-consistency condition (4.3) to determine the gap function. As previously, $\hat{g}$ need only be computed to terms of $O(\Delta)$ for determining T_c. Further simplifications arise from the form of the single-impurity diagrams G_f and F_f in the CS limit [Eq. (B5)].

One requires only contributions to V^2G_f and $V^4\Gamma_f$ of $O(V^4)$ and lower. To this order, three diagrams appear in G_f and a single diagram in Γ_f; these are collected in Fig. 18. The partition function Z_f is just

$$\begin{aligned} Z_f&=\int\frac{dz}{2\pi i}e^{-\beta z}\left[\frac{1}{z}+\frac{N}{z-\varepsilon_f}\right]+O(V^2) \\ &=1+Ne^{-\beta\varepsilon_f}+O(V^2)\ . \end{aligned} \tag{B6}$$

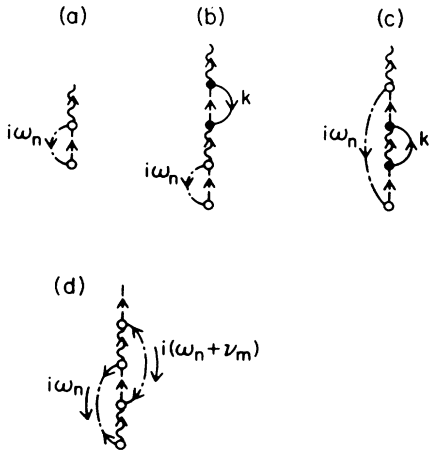

FIG. 18. Contributions to the normal Green's function G_f and impurity scattering vertex Γ_f for calculation for T_c depression to $O(V^4)$. (a) Lowest-order contribution to G_f. (b) and (c) $O(V^2)$ contributions to G_f. (d) Lowest-order contribution to Γ_f.

Figure 18(a) is evaluated as

$$\begin{aligned} V^2G_f^{(1)}(i\omega_n)&=\frac{V^2}{Z_f}\int\frac{dz}{2\pi i}e^{-\beta z}\frac{1}{z+i\omega_n-\varepsilon_f}\frac{1}{z} \\ &=\left[\frac{1+e^{-\beta\varepsilon_f}}{1+Ne^{-\beta\varepsilon_f}}+O(V^2)\right]\frac{V^2}{i\omega_n-\varepsilon_f}\ . \end{aligned} \tag{B7a}$$

Thus, in the CS limit,

$$V^2G_f^{(1)}(i\omega_n)=-\frac{J}{N}+O(J^2)\ . \tag{B7b}$$

The second contribution arises from the partition function. This entire term is real valued and does not contribute to $(-dT_c/dC)\,|_{C=0}$. Hence, the $O(J^2)$ term need not be calculated.

Since Figs. 18(b)–18(d) are $O(V^4)$, only the $O(1)$ contribution to the partition function need be retained in their evaluation. Figure 18(b) yields

$$\begin{aligned} V^2G_f^{(2)}(i\omega_n)&=\frac{NV^4}{Z_f}\int\frac{dz}{2\pi i}e^{-\beta z}\frac{1}{z+i\omega_n-\varepsilon_f}\frac{1}{z^2}\sum_k\frac{f_k}{z+\varepsilon_k-\varepsilon_f} \\ &=\frac{NV^4}{1+Ne^{-\beta\varepsilon_f}}\left[e^{-\beta\varepsilon_f}\sum_k\frac{f_k}{i\omega_n-\varepsilon_k}\left[\frac{e^{\beta\varepsilon_k}}{(\varepsilon_f-\varepsilon_k)^2}+\frac{1}{(i\omega_n-\varepsilon_f)^2}\right]+O((e^{-\beta\varepsilon_f})^0)\right]\ , \end{aligned} \tag{B8a}$$

which reduces in the CS limit to

$$V^2G_f^{(2)}(i\omega_n)=J^2\sum_k\frac{1}{i\omega_n-\varepsilon_k}=-iJ^2N(0)\pi(\text{sgn}\omega)+\mathcal{R}\ , \tag{B8b}$$

where $\mathcal{R}$ is a real constant. By a parallel calculation, one finds for Fig. 18(c)

$$\begin{aligned} V^2G_f^{(3)}(i\omega_n)&=\frac{V^4}{Z_f}\int\frac{dz}{2\pi i}e^{-\beta z}\frac{1}{(z+i\omega_n-\varepsilon_f)^2} \\ &\quad\times\sum_k\frac{1-f_k}{z+i\omega_n-\varepsilon_k z}\frac{1}{z} \\ &\to\frac{J^2}{NT}\sum_k(1-f_k)=\mathcal{R}\ . \end{aligned} \tag{B9}$$

Consider finally Fig. 18(d). Substituting for $\hat{g}_0^{12}$ from Eq. (6.7) gives

$$V^2F_f^{(1)}(i\omega_n)=\pi N(0)V^4\Delta\frac{1}{\beta}\sum_m\frac{\Gamma_f(i\omega_n,i\nu_m)}{|\omega_n+\nu_m|}\ ,$$

with

$$\Gamma_f(i\omega_n,i\nu_m)\equiv\frac{1}{Z_f}\int_\Gamma\frac{dz}{2\pi i}e^{-\beta z}\frac{1}{z-\varepsilon_f}\frac{1}{z+i(\omega_n+\nu_m)}\times\frac{1}{z+i\omega_n}\frac{1}{z+i(2\omega_n+\nu_m)-\varepsilon_f}\ . \tag{B10a}$$

One finds upon passage to the CS limit

$$V^4\Gamma_f(i\omega_n,i\nu_m)=\begin{cases}0, & \nu_m\neq-2\omega_n\\ -J^2/NT, & \nu_m=-2\omega_n\ .\end{cases} \tag{B10b}$$

Hence,

$$V^2F_f^{(1)}(i\omega_n)=-\frac{\Delta\pi N(0)J^2}{N|\omega_n|}\ . \tag{B10c}$$

The quasiclassical propagator $\hat{g}$ may now be computed to terms of $O(\Delta)$. In this case, one must solve the Eilenberger equation

$$[i\omega_n\hat{\tau}_3-\Delta(i\sigma_2)\tau_1,\hat{g}(i\omega_n)]=C[\hat{t}(i\omega_n),\hat{g}(i\omega_n)]\ ,\qquad \hat{g}^2(i\omega_n)=-\pi^2\hat{1}\ , \tag{B11a}$$

where $\hat{t}(i\omega_n)$ is to be determined self-consistently, i.e.,

$$\hat{t}(i\omega_n)=\hat{t}\{\hat{g}(i\omega_n)\}\equiv\mathrm{Re}\,t_1(i\omega_n)\hat{1}+i\,\mathrm{Im}\,t_1(i\omega_n)\hat{\tau}_3+t_2(i\omega_n)(i\sigma_2)\hat{\tau}_1\ . \tag{B11b}$$

This may be accomplished by making the replacement

$$i\omega_n\to i\tilde{\omega}_n(\omega_n)=i[\omega_n-C\,\mathrm{Im}\,t_1(i\tilde{\omega}_n,\tilde{\Delta})]\ ,\qquad \Delta\to\tilde{\Delta}(\omega_n)=\Delta+Ct_2(i\tilde{\omega}_n,\tilde{\Delta})\ , \tag{B12a}$$

and solving the equation

$$[i\tilde{\omega}_n\hat{\tau}_3-\tilde{\Delta}(i\sigma_2)\hat{\tau}_1,\hat{g}(i\omega_n)]=0\ . \tag{B12b}$$

This equation has the linearized solution

$$\hat{g}(i\omega_n)=-\frac{\pi}{|\tilde{\omega}_n|}[i\tilde{\omega}_n\hat{\tau}_3-i\tilde{\Delta}(i\sigma_2)\hat{\tau}_1]\ . \tag{B13}$$

The quantities $\tilde{\omega}_n$ and $\tilde{\Delta}$ may now be determined from the self-consistent equation for $\hat{t}$. One finds from Eqs. (6.11) and (B6)–(B10) that

$$C\hat{t}(i\omega_n)=(-i\,\mathrm{sgn}\,\tilde{\omega}_n)(\tfrac{1}{2}\tau_1^{-1})\hat{\tau}_3-\frac{\tilde{\Delta}}{|\tilde{\omega}_n|}(i\sigma_2)(\tfrac{1}{2}\tau_2^{-1})\hat{\tau}_1\ ,$$

where

$$\tfrac{1}{2}\tau_1^{-1}=\frac{2j+1}{2}C\pi N(0)J^2\ ,\qquad \tfrac{1}{2}\tau_2^{-1}=\tfrac{1}{2}C\pi N(0)J^2\ . \tag{B14}$$

Thus,

$$\tilde{\omega}_n=\omega_n+\tfrac{1}{2}\tau_1^{-1}\mathrm{sgn}\,\tilde{\omega}_n\ ,\qquad \tilde{\Delta}=\Delta-\frac{\tilde{\Delta}}{|\tilde{\omega}_n|}\tfrac{1}{2}\tau_2^{-1}\ ,$$

i.e., (B15)

$$|\tilde{\omega}_n|=|\omega_n|+\tfrac{1}{2}\tau_1^{-1}\ ,\qquad |\tilde{\Delta}|=\frac{\Delta|\tilde{\omega}_n|}{|\tilde{\omega}_n|+\tfrac{1}{2}\tau_2^{-1}}\ .$$

The self-consistency condition is now

$$\Delta(i\sigma_2)=\lambda T_c\sum_n\hat{g}^{12}(i\omega_n)\ ,$$

i.e.,

$$1=\lambda T_c\sum_n\frac{\pi}{|\omega_n|+\tfrac{1}{2}\tau_s^{-1}}\ , \tag{B16}$$

with

$$\tfrac{1}{2}\tau_s^{-1}=\tfrac{1}{2}\tau_1^{-1}+\tfrac{1}{2}\tau_2^{-1}=C(j+1)\pi N(0)J^2\ .$$

Performing the sum in (B16) gives finally

$$\ln(T_{c0}/T_c)=\pi T_c\sum_n\left[\frac{1}{|\omega_n|}-\frac{1}{|\omega_n|+\tfrac{1}{2}\tau_s^{-1}}\right]=\psi(\tfrac{1}{2}+\rho)-\psi(\tfrac{1}{2})\ , \tag{B17a}$$

where the pair-breaking parameter

$$\rho=(\pi\tau_sT_c)^{-1} \tag{B17b}$$

and ψ is the digamma function. For $C\to0$, Eq. (B17) reduces to

$$(-dT_c/dC)|_{C=0}=\frac{\pi^2}{4}(j+1)J^2N(0)\ . \tag{B18}$$

This expression disagrees with the result obtained by Coqblin and Schrieffer in their original paper,[27] where the corresponding expression has

$$j+1\to\frac{8j(j+1)}{(2j+1)^2}\ . \tag{B19a}$$

Note that

$$j+1=\frac{8j(j+1)}{(2j+1)^2}=\frac{3}{2} \tag{B19b}$$

for $j=\frac{1}{2}$ (the spin-$\frac{1}{2}$ Kondo model). The original CS result follows from an incorrect *a priori* assumption on the relation between τ_1^{-1} and τ_2^{-1}. (Note that the values of τ_1^{-1} and τ_2^{-1} deduced directly from the CS Hamiltonian [Eq. (B2)] depend on whether a direct scattering term is included; the sum $\tau_1^{-1}+\tau_2^{-1}=\tau_s^{-1}$ is independent of such a term.)

APPENDIX C: EVALUATION OF THE NORMAL AND ANOMALOUS IMPURITY GREEN'S FUNCTIONS

In this appendix, we establish a set of diagrammatic rules for evaluating the impurity Green's functions

$$G_f(MM';i\omega_n)=\int_0^\beta d\tau\, e^{i\omega_n\tau}[-\langle T_\tau F_M(\tau)F_{M'}^\dagger(0)\rangle] \tag{C1}$$

and

$$F_f(MM';i\omega_n)=\int_0^\beta d\tau\, e^{i\omega_n\tau}[-\langle T_\tau F_M(\tau)F_{M'}(0)\rangle] ,$$

where

$$F_M=|0\rangle\langle M| .$$

We discuss F_f in some detail, since its treatment is more complex, then briefly state the analogous rules for evaluating G_f. We follow the general method for treating systems with strong local correlations.[29]

First note that for $\tau>0$,

$$F_f(MM';\tau)=-\frac{1}{Z/Z_0}\left[\frac{1}{Z_0}\mathrm{Tr}\, e^{-\beta H}F_M(\tau)F_{M'}(0)\right] \tag{C2}$$

with

$$Z_0=Z_{\mathrm{band}}(1+Ne^{-\beta\varepsilon_f}) .$$

The quantity in large parentheses may be written out in the interaction representation as a sum of iterated integrals in imaginary time:

$$\frac{1}{Z_0}\mathrm{Tr}\, e^{-\beta H}F_M(\tau)F_{M'}(0)=\sum_{N=1}^{\infty}\sum_{L<N}(-1)^N\int_{\tau_1,\ldots,\tau_L}\int_{\tau_{L+1},\ldots,\tau_N}\langle H_{\mathrm{mix}}(\tau_1)\cdots H_{\mathrm{mix}}(\tau_L)F_M(\tau)$$

$$\times H_{\mathrm{mix}}(\tau_{L+1})\cdots H_{\mathrm{mix}}(\tau_N)F_{M'}(0)\rangle_0$$

with

$$\begin{aligned}
&\langle\hat{O}\rangle_0\equiv Z_0^{-1}\mathrm{Tr}\, e^{-\beta H_0}\hat{O} ,\\
&\hat{O}(\tau)\equiv e^{\tau H_0}\hat{O}e^{-\tau H_0} ,\\
&\int_{\tau_1,\ldots,\tau_L}\equiv\int_\tau^\beta d\tau_1\int_\tau^{\tau_1}d\tau_2\cdots\int_\tau^{\tau_{L-1}}d\tau_L ,\\
&\int_{\tau_{L+1},\ldots,\tau_N}\equiv\int_0^\tau d\tau_{L+1}\int_0^{\tau_{L+1}}d\tau_{L+2}\cdots\int_0^{\tau_{N-1}}d\tau_N .
\end{aligned} \tag{C3}$$

Here, $L<N$ is the number of time points τ_i greater than τ. Only even values of N contribute to the sum.

We may restrict attention to a single choice of N and L. The thermal average in (C3) may then be split into f-electron and conduction-electron components. The f component may be treated first: Since $F_{M'}$ annihilates all states but $|M'\rangle$, this component is, schematically,

$$\frac{e^{-\beta\varepsilon_f}}{1+Ne^{-\beta\varepsilon_f}}\langle M'|F^\dagger(\tau_1)F(\tau_2)\cdots F^\dagger(\tau_L)F_M(\tau)F^\dagger(\tau_{L+1})\cdots F^\dagger(\tau_N)F_{M'}(0)|M'\rangle$$

$$=\frac{e^{-\beta\varepsilon_f}}{1+Ne^{-\beta\varepsilon_f}}\exp[\beta\varepsilon_f(\tau_1-\tau_2+\cdots+\tau_L-\tau+\tau_{L+1}-\cdots+\tau_N)] . \tag{C4}$$

(The labels on the intermediate projection operators are omitted for clarity.)

The conduction-electron component may be evaluated by Wick's theorem. The only nonvanishing contributions linear in the order parameter Δ have exactly $\frac{1}{2}N-1$ creation operators and $\frac{1}{2}N+1$ destruction operators. The extra destruction operators must be paired to give an anomalous expectation value of the form

$$\begin{aligned}
\langle c_{k_iM_i}(\tau_i)c_{k_jM_j}(\tau_j)\rangle&=-\langle T_\tau c_{k_jM_j}(\tau_j)c_{k_iM_i}(\tau_i)\rangle\quad(\tau_i>\tau_j)\\
&=\int\frac{d\hat{\mathbf{k}}_i d\hat{\mathbf{k}}_j}{(4\pi)^2}\alpha^\dagger(M_j;\hat{\mathbf{k}}_j)\hat{G}^{12}(\mathbf{k}_j;\tau_j-\tau_i)\delta_{\mathbf{k}_j,-\mathbf{k}_i}\alpha^*(M_i;\hat{\mathbf{k}}_i)\\
&=\frac{1}{\beta}\sum_n e^{-i\omega_n(\tau_j-\tau_i)}\delta_{k_ik_j}\int\frac{d\hat{\mathbf{k}}}{4\pi}\alpha^\dagger(M_j;\hat{\mathbf{k}})\hat{G}^{12}(\mathbf{k};i\omega_n)\alpha^*(M_i;-\hat{\mathbf{k}}) ,
\end{aligned} \tag{C5}$$

with $\hat{G}$ as in Eq. (4.1) and α as in (5.6) Summing over all values of k_i and k_j and attaching the associated factors of V gives

$$V^2 \sum_{k_i,k_j} \langle c_{k_i M_i}(\tau_i) c_{k_j M_j}(\tau_j) \rangle = \frac{1}{\beta} \sum_n K(M_j M_i; i\omega_n) e^{-i\omega_n(\tau_j - \tau_i)} ,$$

where

$$K(M_j M_i; i\omega_n) = N(0) V^2 \int \frac{d\hat{\mathbf{k}}}{4\pi} \alpha^\dagger(M_j; \hat{\mathbf{k}}) \hat{g}_0^{12}(\hat{\mathbf{k}}; i\omega_n) \times \alpha^*(M_i; -\hat{\mathbf{k}}) , \quad \text{(C6)}$$

and $\hat{g}_0$ is the quasiclassical propagator of Eq. (A2).

It is easy to see that the sets $\{M_i, M_j\}$ and $\{M, M'\}$ must be the same. Exactly $N+2$ impurity projection operators appear in each term of Eq. (C3). Four of these operators, with quantum numbers M, M', M_i, and M_j correspond to the times τ, 0, τ_i, and τ_j. The other $N-2$ operators may be grouped into $\frac{1}{2}N-1$ pairs, connected by the contraction of conduction operators with equal angular momentum. Since angular momentum is "conserved" in the thermal average, the sets $\{M_i M_j\}$ and $\{M, M'\}$ are identical. It may be checked using the definitions of Sec. V that

$$K(M'M; i\omega_n) = -K(MM'; i\omega_n) ; \quad \text{(C7a)}$$

hence,

$$V^2 \sum_{k_i,k_j} \langle c_{k_i M_i}(\tau_i) c_{k_j M_j}(\tau_j) \rangle = (-1)^g \frac{1}{\beta} \sum_n K(MM'; i\omega_n) e^{-i\omega_n(\tau_j - \tau_i)} , \quad \text{(C7b)}$$

where

$$g = \begin{cases} 0 & \text{if } M = M_j , \\ 1 & \text{if } M' = M_j . \end{cases} \quad \text{(C7c)}$$

It is simplest to separate out the time dependence of all other conduction operators in (C3) by noting that

$$c_{kM}(\tau) = e^{-\tau\varepsilon_k} c_{k,M} , \qquad c^\dagger_{kM}(\tau) = e^{\tau\varepsilon_k} c^\dagger_{kM} . \quad \text{(C8)}$$

The remaining operators in the conduction average may then be contracted to give products of Fermi functions. The time dependence from Eq. (C7b) is the same as that arising from a destruction operator with "energy" $i\omega_n$ at τ_j and a creation operator with the same energy at τ_i, where $\tau_i > \tau_j$.

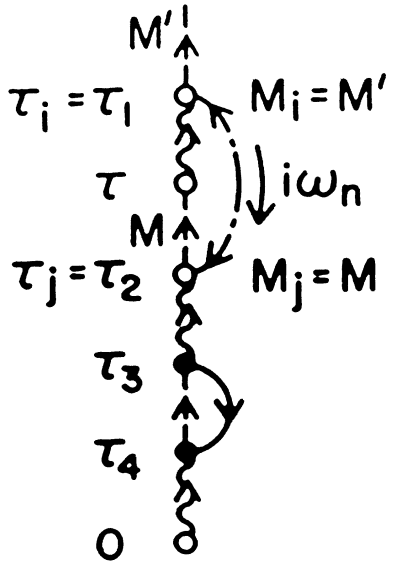

FIG. 19. Example for contraction of conduction operators by Wick's theorem. In this case, $N=4$ (since four factors of the interaction Hamiltonian appear), and $L=1$ (since only one time point is larger than τ). Conduction-electron destruction operators at $\tau_i=\tau_1$ and $\tau_j=\tau_2$ are contracted to give an anomalous propagator, denoted by a dash-dotted line. A creation operator at τ_3 is contracted with a destruction operator at τ_4 to give a Fermi function $\langle c_k^\dagger c_k \rangle = f_k$.

A contraction for a specified choice of N and L may be represented diagramatically. An example for $N=4$ $L=1$, is shown in Fig. 19. Open circles represent the operators $F_M(\tau)$ and $F_{M'}(0)$ and the end points of the anomalous line; solid dots represent the interaction vertices. Time increases as the diagram is traversed vertically. Normal conduction lines carry energy ε_k; the anomalous conduction line (dash-dotted) carries "energy" $i\omega_n$. A Fermi factor f_k may be associated with each descending conduction line and a factor $1-f_k$ with each ascending conduction line. The overall sign of a contraction follows from the anticommutation relations of the conduction-electron operators. Diagrammatically, the sign is just $(-1)^c$, with c the total number of conduction line crossings. It is also easy to find the constant g in Eq. (C7c). If a continuous path of dashed and solid lines can be traced between the lower anomalous vertex and the upper open circle, $g=0$; otherwise, $g=1$. Thus, a single contribution to (C2) takes the form

$$-\frac{1}{Z_f} e^{-\beta\varepsilon_f} (-1)^{c+g} V^{N-2} \prod_{a,d} (1-f_{k_a}) f_{k_d} \frac{1}{\beta} \sum_n K(MM'; i\omega_n) (-1)^N e^{-\varepsilon_f \tau} \int_{\tau_1,\ldots,\tau_L} \int_{\tau_{L+1},\ldots,\tau_N} F(\{\tau_i\}) , \quad \text{(C9)}$$

where lines with momentum k_a (k_d) are ascending (descending), and F is a product of imaginary time exponentials dependent on f- and conduction-electron energies and $i\omega_n$ (the energy of the anomalous line).

The iterated integral

$$\int_{\tau_{L+1},\ldots,\tau_N} \tag{C10}$$

may be simply evaluated by (a) introducing the difference variables

$$\begin{aligned} u_i &= \tau_i - \tau_{i+1}, \quad i = L+1, \ldots, N-1 \\ u_N &= \tau_N \ , \end{aligned} \tag{C11}$$

and (b) noting that for $a < 0$,

$$\int_{a+i\infty}^{a-i\infty} \frac{dz}{2\pi i} \frac{e^{z(\tau_{L+1}-\tau)}}{z} = \begin{cases} 0, & \tau_{L+1} > \tau \\ 1, & \tau_{L+1} < \tau \ . \end{cases} \tag{C12}$$

Thus,

$$\int_{\tau_{L+1},\ldots,\tau_N} F(\{\tau_i\}) = \int_{a+i\infty}^{a-i\infty} \frac{dz}{2\pi i} \frac{e^{-z\tau}}{z} \int_0^\infty du_{L+1} \cdots \int_0^\infty du_N \exp\left[z \sum_{n=L+1}^{N} u_n \right] F(\{u_i\}) \ . \tag{C13}$$

(The upper limits of integration for the u_i may always be extended to ∞ if a is chosen sufficiently negative to insure convergence.) The function F may be written out explicitly as

$$F(\{\tau_i\}) = \prod_{i=L+1}^{N} \exp(\tau_i \Delta E_i) \ , \tag{C14}$$

where ΔE_i is the total energy of f- and conduction-electron excitations created at time τ_i; for example, if an f electron is created and a conduction electron of energy ε_k is destroyed, then $\Delta E_i = \varepsilon_f - \varepsilon_k$. Since

$$\tau_j = \sum_{n=j}^{N} u_n \ , \tag{C15}$$

it follows that

$$F(\{u_i\}) = \prod_{i=L+1}^{N} \exp(-u_i \mathcal{E}_i) \ , \tag{C16}$$

with

$$\mathcal{E}_i = -\sum_{n=L+1}^{i} \Delta E_i, \quad i = L+1, \ldots, N \ .$$

Thus,

$$\int_{\tau_{L+1},\ldots,\tau_N} \prod_{i=L+1}^{N} \exp(\tau_i \Delta E_i)$$

$$= (-1)^{N-L} \int_{a+i\infty}^{a-i\infty} \frac{dz}{2\pi i} \frac{e^{-\tau z}}{z} \prod_{i=L+1}^{N} \frac{1}{z - \mathcal{E}_i} \ . \tag{C17}$$

In similar fashion, it is easy to show that

$$\int_{\tau_1,\ldots,\tau_L} \prod_{i=1}^{L} \exp(\tau_i \Delta E_i)$$

$$= (-1)^L \int_{b+i\infty}^{b-i\infty} \frac{dz'}{2\pi i} \frac{e^{-\beta z'}}{z'} e^{\tau(z' - \bar{\mathcal{E}}_L)} \prod_{i=1}^{L} \frac{1}{z' - \bar{\mathcal{E}}_i} \ ,$$

with

$$\bar{\mathcal{E}}_i = -\sum_{n=1}^{i} \Delta E_n, \quad i = 1, \ldots, L \ . \tag{C18}$$

The negative real numbers a and b may be chosen such that

$$b > a + (\bar{\mathcal{E}}_L + \varepsilon_f) \ . \tag{C19}$$

The reason for this choice appears shortly.

The Fourier transform of a single contribution to (C2) may now be written out as

$$-\frac{1}{Z_f} e^{-\beta\varepsilon_f} (-1)^{c+g} V^{N-2} \prod_{a,d} (1 - f_{k_a}) f_{k_d} \frac{1}{\beta} \sum_{n'} K(MM'; i\omega_{n'}) \int_{a+i\infty}^{a-i\infty} \frac{dz}{2\pi i} \int_{b+i\infty}^{b-i\infty} \frac{dz'}{2\pi i} \frac{e^{-\beta z'}}{zz'}$$

$$\times \int_0^\beta d\tau \exp[(i\omega_n - z + z' - \varepsilon_f - \bar{\mathcal{E}}_L)\tau] \prod_{i=1}^{L} \frac{1}{z' - \bar{\mathcal{E}}_i} \prod_{j=L+1}^{N} \frac{1}{z - \mathcal{E}_j} \ . \tag{C20}$$

The integral over τ gives simply

$$-\frac{e^{\beta z'}}{i\omega_n - z + z' - \varepsilon_f - \bar{\mathcal{E}}_L} (e^{-\beta z} e^{-\beta(\varepsilon_f + \bar{\mathcal{E}}_L)} + e^{-\beta z'}) \ . \tag{C21}$$

Thus, two terms, proportional to $e^{-\beta z}$ and $e^{-\beta z'}$, appear in the double contour integral. The term proportional to $e^{-\beta z}$ may be integrated over z' by closing the contour to the left. There are no singularities in this region [since $b < a + (\bar{\mathcal{E}}_L + \varepsilon_f)$], and the integral vanishes. The term containing $e^{-\beta z'}$ may be integrated over z by closing the contour to the left. In this case, there is a single pole at

$$z = i\omega_n + z' - (\varepsilon_f + \bar{\mathcal{E}}_L) \ . \tag{C22}$$

Thus, the contribution to F from Eq. (C20) becomes

$$\frac{1}{Z_f}e^{-\beta\varepsilon_f}(-1)^{c+g}V^{N-2}\prod_{a,d}(1-f_{k_a})f_{k_d}\frac{1}{\beta}\sum_{n'}K(MM';i\omega_{n'})\int_{b+i\infty}^{b-i\infty}\frac{dz}{2\pi i}\frac{e^{-\beta z}}{z}\prod_{i=1}^{L}\frac{1}{z-\bar{\mathcal{E}}_i}\frac{1}{z+i\omega_n-(\varepsilon_f+\bar{\mathcal{E}}_L)}$$
$$\times\prod_{j=L+1}^{N}\frac{1}{z+i\omega_n-(\mathcal{E}_j+\varepsilon_f+\bar{\mathcal{E}}_L)}\ . \tag{C23}$$

The path of integration may now be distorted into a contour Γ which encircles all singularities of the integrand in a counterclockwise fashion. In addition, it is convenient to shift the variable of integration by $z\to z-\varepsilon_f$. The energy denominators in the resulting expression may be given a simple diagrammatic interpretation. The steps are the following: (a) Add to the diagrams generated from the contraction of conduction operators (e.g., Fig. 19) an external line, which carries "energy" $i\omega_n$, connecting the remaining open circles (it is convenient to draw this line to the left of the diagram to prevent confusion with conduction electron lines); (b) assign a factor $(z-E_\alpha)^{-1}$ to the interval between each pair of vertices. E_α is found by adding the energies of all lines ascending between the vertices and subtracting the energies of all lines descending. A general contribution to F may then be written down following the rules summarized in Table IV. For example, the diagram of $O(V^4)$ in Fig. 20 gives

$$\frac{1}{\beta}\sum_m K(MM';i(\omega_n+\nu_m))\frac{1}{Z_f}V^2\sum_k(1-f_k)\int_\Gamma\frac{dz}{2\pi i}e^{-\beta z}\frac{1}{z-\varepsilon_f}$$
$$\times\frac{1}{z-\varepsilon_k}\frac{1}{z+i\omega_n-\varepsilon_f-\varepsilon_k}\frac{1}{z+i(2\omega_n+\nu_m)-\varepsilon_k}\frac{1}{z+i(2\omega_n+\nu_m)-\varepsilon_f}\frac{1}{z+i\omega_n}\ . \tag{C24}$$

Note that in this case $c=g=1$.

The normal Green's function G_f may be evaluated in a completely analogous way. The treatment is somewhat simpler, since only normal-state contributions need be considered; the leading anomalous contributions are $O(\Delta^2)$. We simply summarize the rules for evaluating G_f in Table II.

APPENDIX D: REDUCTION OF MATSUBARA SUMS

The initial slope of T_c depression $(-dT_c/dC)\,|_{C=0}$ has been expressed in terms of two Matsubara sums in Eq. (6.12). These sums are reduced to spectral integrals below.

The sum

$$S_1(T)=T^2\sum_n \mathrm{Im}\,G_f(i\omega_n)\frac{\mathrm{sgn}\,\omega_n}{\omega_n^2}\ , \tag{D1}$$

which arises in Eq. (6.12), may be evaluated by employing a spectral representation for the dressed propagator:

$$G_f(i\omega_n)=\int_{-\infty}^{\infty}d\epsilon\frac{\rho_f(\epsilon)}{i\omega_n-\epsilon}\ , \tag{D2}$$

with $\rho_f(\epsilon)$ as in Eq. (6.17). Thus,

$$S_1(T)=-\int_{-\infty}^{\infty}d\epsilon\,\rho_f(\epsilon)R_1(\epsilon)\ , \tag{D3}$$

where

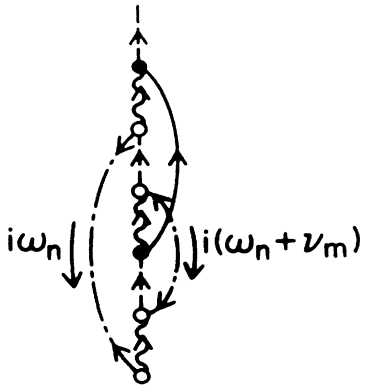

FIG. 20. Example for evaluating F_f. (This example is worked out in step-by-step detail in Fig. 15.) The single conduction line crossing contributes a factor of -1; since a continuous path of dashed and solid lines *cannot* be traced between the lower anomalous vertex and the upper factor of F_M, the diagram receives an additional factor of -1.

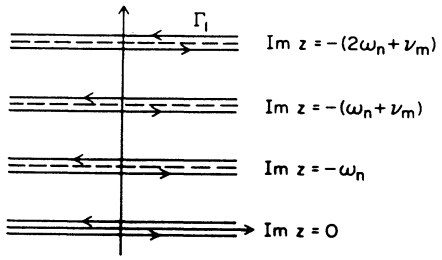

FIG. 21. Contour of integration Γ_1 encircling all singularities of the integrand in (D6) in a counterclockwise fashion.

$$R_1(\epsilon) = -T^2 \,\mathrm{Im} \sum_n \frac{1}{i\omega_n - \epsilon} \frac{\mathrm{sgn}\,\omega_n}{\omega_n^2}$$

$$= T^2 \sum_n \frac{1}{|\omega_n|} \frac{1}{\omega_n^2 + \epsilon^2}$$

$$= -\frac{T}{\pi\epsilon^2} \left[\psi(\tfrac{1}{2}) - \mathrm{Re}\,\psi \left[\frac{1}{2} + \frac{i\epsilon}{2\pi T} \right] \right] . \quad \text{(D4)}$$

Consider now the more complex sum [Eqs. (6.9) and (6.12)]

$$S_2(T) = T^3 \sum_{n,m} \frac{\Gamma_f(i\omega_n, i\nu_m)}{|\omega_n|\,|\omega_n + \nu_m|} , \quad \text{(D5)}$$

where

$$\Gamma_f(i\omega_n, i\nu_m) = \frac{1}{Z_f} \int_{\Gamma_1} \frac{dz}{2\pi i} e^{-\beta z} G_M(z) G_0(z + i(\omega_n + \nu_m))$$

$$\times G_M(z + i(2\omega_n + \nu_m))$$

$$\times G_0(z + i\omega_n) , \quad \text{(D6)}$$

with Γ_1 as in Fig. 21. Introducing the densities ρ_0 and ρ_M of Eq. (6.16) gives

TABLE IV. Diagrammatic rules for evaluating $F_f(i\omega_n)$. We list below rules for evaluating the anomalous f Green's function $F_f(i\omega_n)$ to lowest order in the pairing amplitude Δ.

To compute a general contribution to $F_f(MM';i\omega_n)$ of $O(V^{2n},\Delta)$, $n \geq 1$.

(a) Set down $2n+2$ vertices (solid circles) in a vertical line. Beginning at the bottom with a wavy line, connect the vertices with alternating wavy and dashed lines (all ascending), finally leaving the highest vertex on a dashed line. (A total of $2n+2$ lines now appear.)

(b) Convert four vertices to open circles, representing the operators F_M and $F_{M'}$ and the two points at which an anomalous conduction line is to be attached: counting from the bottom, convert the first vertex (to represent $F_{M'}$), one other odd-numbered vertex (to represent F_M), and two even-numbered vertices (the points of attachment for the anomalous line).

(c) Always working to the right of the vertical line, connect the remaining $2n-2$ vertices with solid lines in all possible ways which maintain the direction of the dashed line at each vertex.

(d) Working on the left-hand side of the diagram, connect the open circles at odd-numbered points with a dash-dotted "external line." This line carries angular momentum M into the top circle, M' into the bottom circle, and "energy" $i\omega_n$ from top to bottom.

(e) Working on the right-hand side of the diagram, connect the remaining open circles (at even-numbered vertices) with a dash-dotted line, representing the anomalous conduction propagator

$$K(MM';i(\omega_n+\nu_m)) = N(0)V^2 \int \frac{d\hat{\mathbf{k}}}{4\pi} \alpha^\dagger(M;\hat{\mathbf{k}}) \hat{g}_0^{12}(\hat{\mathbf{k}};i(\omega_n+\nu_m)) \alpha^*(M';-\hat{\mathbf{k}}) = \frac{\Gamma\Delta}{|\omega_n+\nu_m|} \delta_{M,-M'} (-1)^{j+M} .$$

The "energy" $i(\omega_n+\nu_m)$ flows from top to bottom.

(f) Assign quantum numbers kM (M) to solid lines (dashed lines), conserving angular momentum at each vertex.

(g) Assign to ascending band lines a factor $1-f_{kM}$ and to descending band lines a factor f_{kM}, with f the Fermi function.

(h) Draw a perpendicular to each local configuration line, and assign to it an energy denominator $(z-E_\alpha)^{-1}$, where E_α is found by adding the energies of ascending lines intersected by the perpendicular and subtracting the energies of descending lines intersected.

(i) Multiply the product of energy denominators and Fermi factors by

$$V^{2n-2}(-1)^{c+g} K(MM';i(\omega_n+\nu_m)) .$$

Here, c is the number of line crossings on the right-hand side of the diagram (including the anomalous conduction line); g is 0 if a continuous path of dashed and solid lines can be traced between the lower endpoint of the dashed-dotted line on the right and the upper end point of the dashed-dotted line of the left; and 1 otherwise. Sum on conduction momenta, internal angular momenta, and the Matsubara index m (with an associated factor of $1/\beta$).

(j) Compute the contour integral $(1/Z_f)\int_\Gamma (dz/2\pi i) e^{-\beta z} R(z)$, where R is the result of the preceding operations, Z_f is the system partition function, and Γ encircles all singularities of R in a counterclockwise fashion.

$$\Gamma_f(i\omega_n,i\nu_m)=\frac{1}{Z_f}\int_{-\infty}^{\infty}d\epsilon\, e^{-\beta\epsilon}[\rho_M(\epsilon)G_M(\epsilon-i(2\omega_n+\nu_m))G_0(\epsilon-i(\omega_n+\nu_m))G_0(\epsilon-i\omega_n)$$

$$+\rho_M(\epsilon)G_M(\epsilon+i(2\omega_n+\nu_m))G_0(\epsilon+i\omega_n)G_0(\epsilon+i(\omega_n+\nu_m))$$

$$-\rho_0(\epsilon)G_M(\epsilon+i(\omega_n+\nu_M))G_M(\epsilon-i\omega_n)G_0(\epsilon+i\nu_m)$$

$$-\rho_0(\epsilon)G_M(\epsilon+i\omega_n)G_M(\epsilon-i(\omega_n+\nu_m))G_0(\epsilon-i\nu_m)],\quad \nu_m\neq 0,-2\omega_n\ . \tag{D7}$$

This expression for Γ_f is not valid for $\nu_m=0$ or $-2\omega_n$ (note that these cases are mutually exclusive); in such cases, two of the contours in Fig. 21 become degenerate. The resulting expressions are

$$\Gamma_f(i\omega_n,0)=\frac{1}{Z_f}\int_{-\infty}^{\infty}d\epsilon\, e^{-\beta\epsilon}\{\rho_M(\epsilon)[G_M(\epsilon-2i\omega_n)G_0^2(\epsilon-i\omega_n)+G_M(\epsilon+2i\omega_n)G_0^2(\epsilon+i\omega_n)]$$

$$-2\,\mathrm{Re}\,G_0(\epsilon)\rho_0(\epsilon)G_M(\epsilon+i\omega_n)G_M(\epsilon-i\omega_n)\} \tag{D8a}$$

and

$$\Gamma_f(i\omega_n,-2i\omega_n)=\frac{1}{Z_f}\int_{-\infty}^{\infty}d\epsilon\, e^{-\beta\epsilon}\{2\,\mathrm{Re}\,G_M(\epsilon)\rho_M(\epsilon)G_0(\epsilon+i\omega_n)G_0(\epsilon-i\omega_n)$$

$$-\rho_0(\epsilon)[G_M^2(\epsilon-i\omega_n)G_0(\epsilon-2i\omega_n)+G_M^2(\epsilon+i\omega_n)G_0(\epsilon+2i\omega_n)]\}\ . \tag{D8b}$$

The terms in Eqs. (D8) correspond to elastic and elastic spin-flip scattering. These are the only terms which have been included in numerical calculations to date. They are explicitly reduced to spectral representations at the end of this appendix.

Note now that the first and second (third and fourth) terms in Eq. (D7) are related by the interchange

$$\omega_n\rightarrow-\omega_n,\quad \nu_m\rightarrow-\nu_m\ . \tag{D9a}$$

Further, the first and third (second and fourth) terms are related by a change of sign and the interchange

$$\omega_n\rightarrow-(\omega_n+\nu_m),\quad \nu_m\rightarrow 2\omega_n+\nu_m,\quad M\leftrightarrow 0\ . \tag{D9b}$$

The last notation indicates the interchange of subscripts 0 and M. Finally, note that

$$\Gamma_f(i\omega_n,-2i\omega_n)=-\Gamma_f(i\omega_n,0)\,|_{M\leftrightarrow 0}\ . \tag{D9c}$$

It follows that the series in Eq. (D5) may be resummed to combine terms in the form

$$S_2(T)=\left[\left[T^2\sum_n\frac{\Upsilon(i\omega_n)}{|\omega_n|}+T^3\sum_n\frac{\bar{\Gamma}_f(i\omega_n)}{\omega_n^2}\right]-(M\leftrightarrow 0)\right], \tag{D10a}$$

where

$$\bar{\Gamma}_f(i\omega_n)=\frac{2}{Z_f}\int_{-\infty}^{\infty}d\epsilon\, e^{-\beta\epsilon}\rho_M(\epsilon)G_0(\epsilon-i\omega_n)[G_M(\epsilon-2i\omega_n)G_0(\epsilon-i\omega_n)+\mathrm{Re}\,G_M(\epsilon)G_0(\epsilon+i\omega_n)]\ , \tag{D10b}$$

$$\Upsilon(i\omega_n)=\frac{2}{Z_f}\int_{-\infty}^{\infty}d\epsilon\, e^{-\beta\epsilon}\rho_M(\epsilon)G_0(\epsilon-i\omega_n)\Upsilon_1(i\omega_n;\epsilon)\ , \tag{D10c}$$

with

$$\Upsilon_1(i\omega_n;\epsilon)=T\sum_{m\neq 0,-(2n+1)}\frac{G_M(\epsilon-i(2\omega_n+\nu_m))G_0(\epsilon-i(\omega_n+\nu_m))}{|\omega_n+\nu_m|}\ . \tag{D10d}$$

To aid in the evaluation of Υ_1, we write

$$F(i\nu_m;i\omega_n)\equiv\frac{1}{|\omega_n+\nu_m|}=\begin{cases}i/(i\nu_m+i\omega_n), & \nu_m>-\omega_n\\ -i/(i\nu_m+i\omega_n), & \nu_m<-\omega_n\ .\end{cases} \tag{D11a}$$

This function of $i\nu_m$ may be analytically continued in the complex plane, cut along the line $\mathrm{Im}\,z=-\omega_n$, as

$$F(z;i\omega_n)=\begin{cases} i/(z+i\omega_n), & \mathrm{Im}\, z > -\omega_n \\ -i/(z+i\omega_n), & \mathrm{Im}\, z < -\omega_n \end{cases} . \tag{D11b}$$

The sum in $\Upsilon_1(i\omega_n;\epsilon)$ may now be written as an integral over the contour Γ_2 in Fig. 22:

$$\Upsilon_1(i\omega_n;\epsilon)=\int_{\Gamma_2}\frac{dz}{4\pi i}\coth\left[\frac{z}{2T}\right]G_M(\epsilon-2i\omega_n-z)G_0(\epsilon-i\omega_n-z)F(z;i\omega_n) . \tag{D12}$$

Note that the values 0, $-\omega_n$, and $-2\omega_n$ are always distinct, so the contours never become degenerate. The integral over the arcs at infinity vanishes; noting that

$$F(0;i\omega_n)=F(-2i\omega_n;i\omega_n)=\frac{1}{|\omega_n|} , \tag{D13}$$

one finds

$$\Upsilon_1(i\omega_n;\epsilon)=-T\frac{G_M(\epsilon-2i\omega_n)G_0(\epsilon-i\omega_n)}{|\omega_n|}-T\frac{\mathrm{Re}\, G_M(\epsilon)G_0(\epsilon+i\omega_n)}{|\omega_n|}+\Upsilon_2(i\omega_n;\epsilon) , \tag{D14a}$$

with

$$\Upsilon_2(i\omega_n;\epsilon)=\tfrac{1}{2}\int_{-\infty}^{\infty}d\epsilon_1\left[\coth\left[\frac{\epsilon_1}{2T}\right]\rho_M(\epsilon-\epsilon_1)G_0(\epsilon-\epsilon_1+i\omega_n)\frac{(-i\,\mathrm{sgn}\,\omega_n)}{\epsilon_1-i\omega_n}\right.$$
$$\left.+\tanh\left[\frac{\epsilon_1}{2T}\right]G_M(\epsilon-\epsilon_1-i\omega_n)\,\mathrm{Re}\, G_0(\epsilon-\epsilon_1)\frac{1}{\epsilon_1}\right] . \tag{D14b}$$

A principal value is implied in the vicinity of $\epsilon_1=0$. Note there is no contribution to Υ_1 from the small circle about $z=-i\omega_n$; this is because

$$\coth\left[\frac{-i\omega_n}{2T}\right]=0 . \tag{D15}$$

Substituting the result of Eq. (D14) in Eq. (D10) and noting that the term outside the integral in Υ_1 cancels the contribution from $\overline{\Gamma}_f(i\omega_n)$, one finds

$$S_2(T)=\left[\left[T^2\sum_n\frac{\overline{\Upsilon}(i\omega_n)}{|\omega_n|}\right]-(M\leftrightarrow 0)\right] , \tag{D16a}$$

with

$$\overline{\Upsilon}(i\omega_n)=\frac{2}{Z_f}\int_{-\infty}^{\infty}d\epsilon\, e^{-\beta\epsilon}\rho_M(\epsilon)G_0(\epsilon-i\omega_n)\Upsilon_2(i\omega_n;\epsilon) , \tag{D16b}$$

where Υ_2 is as above.

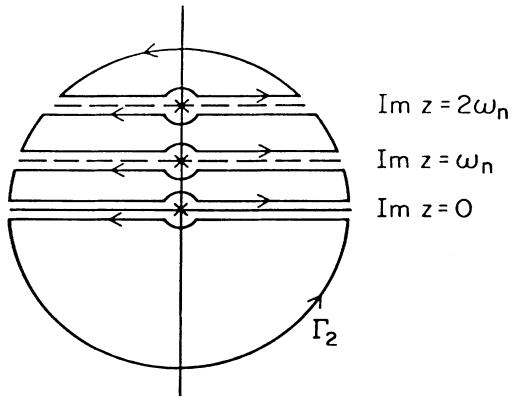

FIG. 22. Contour of integration Γ_2 for performing the Bose frequency sum in Eq. (D10d).

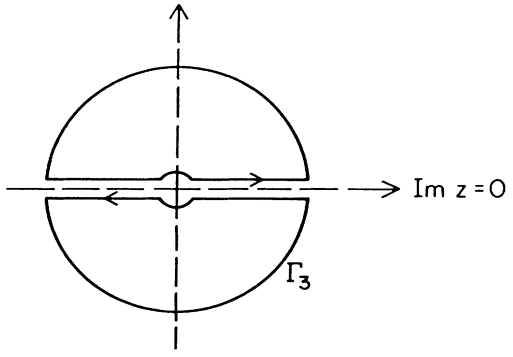

FIG. 23. Contour of integration Γ_3 for the spectral representation of $\overline{\Upsilon}(i\omega_n)$.

Consider now the analytic continuation of $\overline{\Upsilon}(i\omega_n)$ to the complex plane, cut along the real axis. The unique continuation with power-law decay at infinity is obtained by the substitutions

$$i\omega_n \to z \ , \qquad i \operatorname{sgn}\omega_n \to \begin{cases} i, & \mathrm{Im}z > 0 \\ -i, & \mathrm{Im}z < 0 \ . \end{cases} \tag{D17}$$

Applying Cauchy's theorem to the contour in Fig. 23 gives

$$\overline{\Upsilon}(i\omega_n) = \int_{\Gamma_3} \frac{dz}{2\pi i} \frac{\overline{\Upsilon}(z)}{z - i\omega_n} = \int_{-\infty}^{\infty} d\omega \frac{\sigma(\omega)}{i\omega_n - \omega} + I_c \ , \tag{D18a}$$

where

$$\sigma(\omega) = -\frac{1}{\pi} \mathrm{Im}\overline{\Upsilon}(\omega + i0^+) \ , \tag{D18b}$$

I_c is an integral over the small circle, and a principal value is implied in the vicinity of $\omega = 0$. The integral over the small circle is proportion to $(i\omega_n)^{-1}$ and does not contribute to the sum in Eq. (D16a). Hence,

$$S_2(T) = \int_{-\infty}^{\infty} d\omega \left[\left[\sigma(\omega) T^2 \sum_n \frac{1}{|\omega_n|} \frac{1}{i\omega_n - \omega} \right] - (M \leftrightarrow 0) \right] = - \int_{-\infty}^{\infty} d\omega [\sigma(\omega) - (M \leftrightarrow 0)] \omega R_1(\omega) \ , \tag{D19}$$

with R_1 as in Eq. (D4).

From Eq. (D16),

$$\sigma(\omega) = \frac{\pi}{Z_f} \coth\left[\frac{\omega}{2T}\right] \int_{-\infty}^{\infty} d\epsilon \, e^{-\beta\epsilon} \rho_M(\epsilon) \rho_M(\epsilon - \omega) [\rho_0(\epsilon) \mathrm{Re}\, G_0(\epsilon - \omega) - \rho_0(\epsilon - \omega) \mathrm{Re}\, G_0(\epsilon)]$$
$$- \frac{1}{Z_f} \int_{-\infty}^{\infty} d\epsilon \, e^{-\beta\epsilon} \rho_M(\epsilon) \int_{-\infty}^{\infty} d\epsilon_1 \sigma_1(\epsilon, \epsilon_1; \omega) \ , \tag{D20a}$$

with

$$\sigma_1(\epsilon, \epsilon_1; \omega) = \coth\left[\frac{\epsilon_1}{2T}\right] \frac{\rho_M(\epsilon - \epsilon_1)}{\omega - \epsilon_1} [\rho_0(\epsilon - \omega)\rho_0(\epsilon - \epsilon_1 + \omega) + \mathrm{Re}\, G_0(\epsilon - \omega) \mathrm{Re}\, G_0(\epsilon - \epsilon_1 + \omega)]$$
$$+ \tanh\left[\frac{\epsilon_1}{2T}\right] \frac{\mathrm{Re}\, G_0(\epsilon - \epsilon_1)}{\epsilon_1} [\rho_0(\epsilon - \omega) \mathrm{Re}\, G_M(\epsilon - \epsilon_1 - \omega) + \mathrm{Re}\, G_0(\epsilon - \omega) \rho_M(\epsilon - \epsilon_1 - \omega)] \ . \tag{D20b}$$

All integrals above are to be interpreted as principal values in the vicinity of singularities.

The preceding result for the two-particle frequency sums is unwieldy and has not been employed in numerical work. Instead, an "energy-dependent AG approximation" (discussed previously in Sec. VI) has been made, reducing the original sum to

$$S_2(T) \simeq T^3 \sum_{n;m=0,-(2n+1)} \frac{\Gamma_f(i\omega_n, i\nu_m)}{|\omega_n| \, |\omega_n + \nu_m|} = \left[\left[T^3 \sum_n \frac{\Gamma_f(i\omega_n, 0)}{\omega_n^2} \right] - (M \leftrightarrow 0) \right] \ , \tag{D21}$$

with $\Gamma_f(i\omega_n, 0)$ as in Eq. (D8). Since this expression is analytic in the $i\omega_n \to z$ complex plane cut along the real axis, it may be written in a spectral representation. Thus,

$$\Gamma_f(i\omega_n, 0) = \int_{-\infty}^{\infty} d\omega \frac{\sigma_f(\omega)}{i\omega_n - \omega} \ ,$$

where

$$\sigma_f(\omega) = -\frac{1}{\pi} \mathrm{Im} \frac{1}{Z_f} \int_{-\infty}^{\infty} d\epsilon \, e^{-\beta\epsilon} \{ \rho_M(\epsilon) [G_M(\epsilon - 2\omega - i0^+) G_0^2(\epsilon - \omega - i0^+) - G_M(\epsilon + 2\omega + i0^+) G_0^2(\epsilon + \omega + i0^+)]$$
$$- 2 \mathrm{Re}\, G_0(\epsilon) \rho_0(\epsilon) [G_M(\epsilon + \omega + i0^+) G_M(\epsilon - \omega - i0^+)] \} \ , \tag{D22a}$$

i.e.,

$$\sigma_f(\omega)=\frac{1}{Z_f}\int_{-\infty}^{\infty} d\epsilon\, V(\epsilon;\omega)\ ,$$

$$V(\epsilon;\omega)=4\cosh(\omega/2T)e^{-\beta\epsilon}\,\mathrm{Re}\,G_0(\epsilon)\rho_0(\epsilon)[e^{\beta\omega/2}\rho_M(\epsilon-\omega)\,\mathrm{Re}\,G_M(\epsilon+\omega)-e^{-\beta\omega/2}\rho_M(\epsilon+\omega)\,\mathrm{Re}\,G_M(\epsilon-\omega)]$$
$$+2\sinh(\omega/T)e^{-\beta\epsilon}[\,\mathrm{Re}\,G_0^2(\epsilon)-\pi^2\rho_0^2(\epsilon)]\rho_M(\epsilon+\omega)\rho_M(\epsilon-\omega)\ . \tag{D22b}$$

The remaining frequency sum in Eq. (D20) is just

$$T^3\sum_n \frac{1}{\omega_n^2}\frac{1}{i\omega_n-\omega}=-\omega T^3\sum_n \frac{1}{\omega_n^2}\frac{1}{\omega_n^2+\omega^2}$$
$$=-\frac{T}{4\omega}\left[1-\frac{2T}{\omega}\tanh\left[\frac{\omega}{2T}\right]\right]\ . \tag{D23}$$

Thus,

$$S_2(T)\simeq-\int_{-\infty}^{\infty} d\omega[\sigma_f(\omega)-(M\leftrightarrow 0)]R_2(\omega)\ , \tag{D24}$$

with

$$R_2(\omega)=\frac{T}{4\omega}\left[1-\frac{2T}{\omega}\tanh\left[\frac{\omega}{2T}\right]\right]\ .$$

*Present address: Institute for Theoretical Physics, University of California at Santa Barbara, Santa Barbara, CA 93106.
†Present address: Max-Planck-Institut für Festkörperforschung, D-7000 Stuttgart 80, Federal Republic of Germany.

[1]N. E. Bickers, D. L. Cox, and J. W. Wilkins, Phys. Rev. Lett. **54**, 230 (1985); Phys. Rev. B **36**, 2036 (1987); D. L. Cox, N. E. Bickers, and J. W. Wilkins, J. Magn. Magn. Mater. **54-57**, 333 (1986).
[2]H. Keiter and J. C. Kimball, Int. J. Magn. **1**, 233 (1971); N. Grewe, Z. Phys. B **52**, 193 (1982); H. Keiter and G. Czycholl, J. Magn. Magn. Mater. **31**, 477 (1983); Y. Kuramoto, Z. Phys. B **53**, 37 (1983); F. C. Zhang and T. K. Lee, Phys. Rev. B **28**, 33 (1983); P. Coleman, *ibid.* **29**, 3035 (1984).
[3]E. Müller-Hartmann and J. Zittartz, Z. Phys. **256**, 366 (1972).
[4]P. W. Anderson, Phys. Rev. **124**, 41 (1961).
[5]H. R. Krishna-murthy, J. W. Wilkins, and K. G. Wilson, Phys. Rev. B **21**, 1044 (1980); N. Kawakami and A. Okiji, J. App. Phys. **55**, 1931 (1984).
[6]J. R. Schrieffer and P. A. Wolff, Phys. Rev. **149**, 491 (1966).
[7]A. B. Kaiser, J. Phys. C **3**, 410 (1970); H. Shiba, Prog. Theor. Phys. **50**, 50 (1973).
[8]P. Schlottmann, Solid State Commun. **21**, 663 (1977). This work extends the range of validity of Kaiser's theory by use of the renormalization group.
[9]For a list of experimental references, see M. B. Maple, L. E. Delong, and B. C. Sales, in *Handbook on the Physics and Chemistry of Rare Earths,* edited by K. A. Gschneidner, Jr. and L. Eyring (North-Holland, Amsterdam, 1978), p. 797.
[10]P. Schlottmann, J. Low. Temp. Phys. **47**, 27 (1982).
[11]O. Gunnarsson and K. Schönhammer, Phys. Rev. Lett. **50**, 604 (1983); Phys. Rev. B **28**, 4315 (1983).
[12]C. R. Proetto and C. A. Balseiro, Phys. Rev. B **31**, 2847 (1985).
[13]P. W. Anderson, J. Phys. Chem. Solids **11**, 26 (1959).
[14]A. A. Abrikosov and L. P. Gor'kov, Zh. Eksp. Teor. Fiz. **39**, 1781 (1960) [Sov. Phys—JETP **12**, 1243 (1961)].
[15]These arguments apply only for reasonably dilute impurity concentrations in the absence of localization effects.
[16]S. Skalski, O. Betbeder-Matibet, and P. R. Weiss, Phys. Rev. **136**, 1500A (1964).
[17]M. B. Maple, Phys. Lett. **26A**, 513 (1967).
[18]E. Müller-Hartmann, in *Magnetism,* edited by H. Suhl (Academic, New York, 1973), Vol. V, p. 353. This article contains references to the preceding work on the Nagaoka-Hamann equations for superconductors by MHZ and other authors. See also Ref. 3.
[19]Y. Nagaoka, Phys. Rev. **138**, 1112A (1965); D. R. Hamann, *ibid.* **158**, 570 (1967); P. E. Bloomfield and D. R. Hamann, *ibid.* **164**, 856 (1967).
[20]E. Müller-Hartmann and J. Zittartz, Z. Phys. **234**, 58 (1970).
[21]J. Takeuchi and Y. Matsuda, J. Phys. Soc. Jpn. **44**, 402 (1978).
[22]T. Matsuura, S. Ichinose, and Y. Nagaoka, Prog. Theor. Phys. **57**, 713 (1977); T. Matsuura, *ibid.* **57**, 1823 (1977).
[23]A. Sakurai, Phys. Rev. B **17**, 1195 (1978).
[24]E. Müller-Hartmann, Z. Phys. B **57**, 281 (1985); Y. Kuramoto and H. Kojima, *ibid.* **57**, 95 (1984). See also Ref. 1.
[25]A thorough discussion of this method appears in J. W. Serene and D. Rainer, Phys. Rep. **101**, 221 (1983).
[26]E. V. Thuneberg, J. Kurkijärvi, and D. Rainer, J. Phys. C **14**, 5615 (1981).
[27]B. Coqblin and J. R. Schrieffer, Phys. Rev. **185**, 847 (1969).
[28]A. Messiah, *Quantum Mechanics* (North-Holland, Amsterdam, 1961).
[29]H. Keiter and G. Morandi, Phys. Rep. **109**, 227 (1984).
[30]S. E. Barnes, J. Phys. F **6**, 1375 (1976); P. Coleman, Phys. Rev. B **29**, 3035 (1984).
[31]A. A. Abrikosov, Physics **2**, 5 (1965).